

Discovery of ATX968: An Orally Available Allosteric Inhibitor of DHX9

Published as part of *Journal of Medicinal Chemistry special issue "Structural Biology in Drug Discovery and Development"*.

Matthew H. Daniels, Jennifer Castro, Young-Tae Lee, Deepali Gotur, Kevin E. Knockenhauer, Simina Grigoriu, Gordon J. Lockbaum, Jae Eun Cheong, Chuang Lu, David Brennan, Shane M. Buker, Julie Liu, Shihua Yao, Brian A. Sparling,* E. Allen Sickmier, Scott Ribich, Steve J. Blakemore, Serena J. Silver, P. Ann Boriack-Sjodin, Kenneth W. Duncan, and Robert A. Copeland



Cite This: <https://doi.org/10.1021/acs.jmedchem.5c00252>



Read Online

ACCESS |



Metrics & More

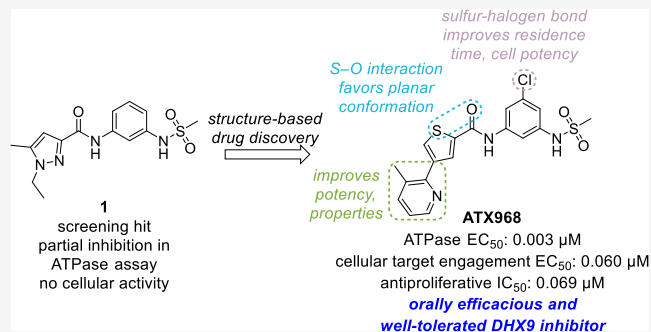


Article Recommendations



Supporting Information

ABSTRACT: DHX9 is an RNA/DNA helicase integral in the maintenance of genome stability that has emerged as an attractive target for oncology drug discovery. Disclosed herein is the discovery and optimization of a series of DHX9 inhibitors. Compound **1** was identified as a partial inhibitor of DHX9 ATPase activity but a full inhibitor of unwinding activity. Binding of **1** to a pocket distinct from the ATP binding site was confirmed by X-ray crystallography, enabling structure-based drug optimization. During this optimization, a sulfur–halogen bond was identified that increased on-target residence time without impacting equilibrium binding affinity. Analysis shows that cell potency more closely correlates with residence time than with equilibrium measurements of binding affinity or biochemical potency. Further optimization of potency and ADME properties led to the identification of **ATX968**, a potent and selective DHX9 inhibitor that is efficacious in a tumor xenograft model of microsatellite instability-high (MSI-H) colorectal cancer.



INTRODUCTION

DHX9 (DEXH-box helicase 9, also known as RNA helicase A (RHA) or nuclear DNA helicase II (NDH II)) is a DEXH-box helicase that plays crucial roles in transcription, translation and the maintenance of genome stability.¹ A key mechanism for achieving these outcomes is unwinding and/or resolving various nucleic acid structures, including double-stranded DNA and RNA, DNA/RNA hybrids (R-loops), circular RNA (circRNA) and G quadruplexes.^{1,2} Genetic ablation of these unwinding activities of DHX9 leads to accumulation of pathological R-loops, which cause transcription collisions at replication forks, resulting in single and double-stranded DNA breaks and increased genome instability.³ Indeed, depletion or chemical inhibition of DHX9 triggers an accumulation of R-loops and markers of replication stress and DNA damage, such as phosphorylation of RPA32 and γ H2AX, respectively, in sensitive tumor cells.⁴ An increase in selective circular RNA (circRNA), a covalently joined continuous single stranded RNA loop specifically generated by Alu element-mediated alternative RNA splicing, has also been observed following DHX9 loss or inhibition and has shown to be a useful biomarker for DHX9 in vivo.^{4–7}

DHX9 is associated with tumorigenesis and its over-expression has been linked to poor survival in a number of cancer types.⁸ Recent publications have revealed a potential role for targeting DHX9 as a cancer therapeutic in tumor types such as small cell lung cancer (SCLC), ovarian cancer, microsatellite instability high (MSI-H) or deficient mismatch repair (dMMR) colorectal cancer (CRC), and gastric and endometrial cancers.^{4,9,10} In addition, suppression of DHX9 via induced knockdown in adult mice is well tolerated with no obvious negative effects after 6 months; these data portend a favorable therapeutic index for inhibitors of DHX9 as molecular targeted cancer therapeutics.¹¹

Genetic knockdown of DHX9 results in strong reduction of proliferation and survival in CRC cells characterized as MSI-

Received: January 24, 2025

Revised: March 21, 2025

Accepted: March 26, 2025

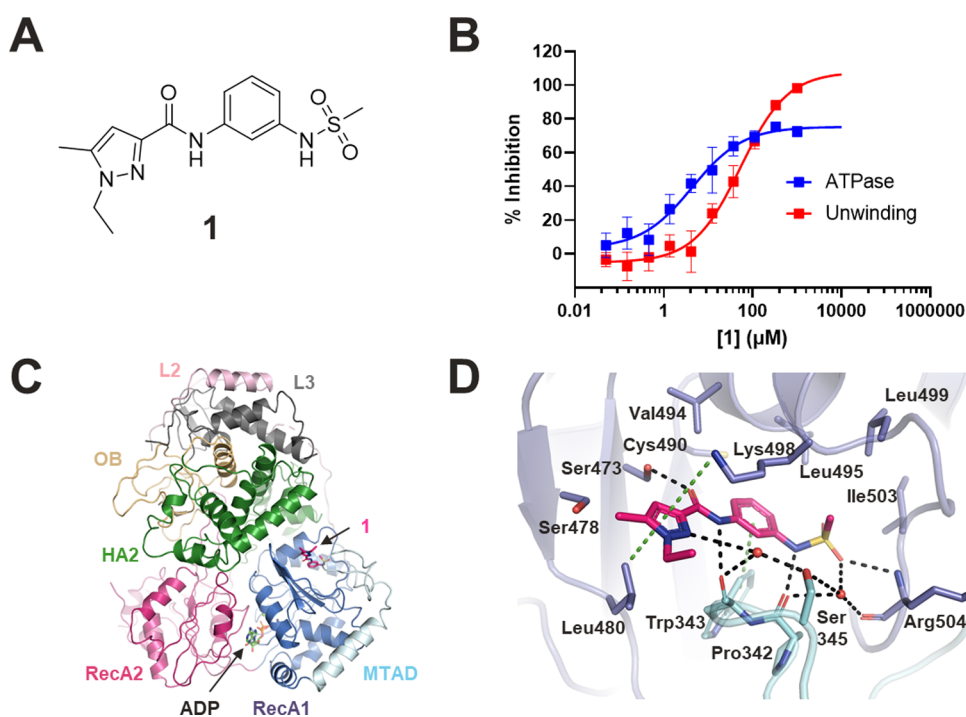


Figure 1. Biochemical and structural properties of **1**. (A) Molecular structure of compound **1**. (B) Concentration–response curves of **1** in ATPase (blue) and unwinding (red) assays. Partial-inhibition behavior (max inhibition 70%) is seen in the ATPase assay and full enzymatic inhibition is seen in the unwinding assay. (C) Crystal structure of **1** (magenta sticks) and ADP (green sticks) bound to feline DHX9 (PDB 9MFP; PDB 8SZQ used as molecular replacement model). DHX9 is shown in cartoon representation and colored by domain. The binding site of **1** is indicated. (D) Zoomed-in view of the binding site of **1** in feline DHX9. **1** has a robust interaction network with DHX9. Residues within 4 Å distance of **1** shown as sticks, water molecules shown as red spheres, hydrogen bonds shown as black dashes, π -stacking interactions shown as green dashes, and other colors as in C.

H/dMMR, but not in microsatellite stable (MSS) CRC cells with proficient MMR (pMMR), demonstrating a selective dependence on DHX9 in MSI-H/dMMR tumors.⁴ Further, the antiproliferative effects of DHX9 knockdown could be rescued by re-expression of wild-type, but not catalytically inactive (K417R) DHX9, demonstrating a selective dependence of DHX9 catalytic activity in MSI-H/dMMR tumors.⁴ Together, these preclinical data validate DHX9 as a tractable and compelling novel oncology target with potential utility as a treatment for cancer patients.

In addition to these genetic studies, treatment with small-molecule inhibitor ATX968 led to robust and durable tumor growth inhibition or regression in mouse xenograft studies with MSI-H/dMMR CRC cell lines but not with MSS/pMMR CRC cell lines, with no concomitant body weight loss in all mice treated.⁴ The work reported here describes the identification and characterization of the initial screening hit **1**, a partial inhibitor of DHX9 ATP hydrolysis but a complete inhibitor of DHX9 unwinding activity, utilizing a bespoke suite of biochemical and biophysical assays.¹² X-ray crystallography showed that compound **1** binds in an allosteric site near the RNA channel exit. Through subsequent medicinal chemistry optimization efforts, in vivo tool compound ATX968 was identified and profiled.

RESULTS AND DISCUSSION

Identification and Characterization of DHX9 Inhibitor

1. To identify potential inhibitors of DHX9, multiple high-throughput screening approaches were undertaken by either binding affinity or functional inhibition. A rigorous process of hit identification, triage and validation utilizing the suite of

assays developed for DHX9¹² was subsequently performed, followed by resynthesis, reconfirmation, initial ADME profiling and medicinal chemistry review. Ultimately, compound **1** (Figure 1A) was identified as a validated DHX9 inhibitor and selected for an optimization campaign.

Close examination of the DHX9 ATPase assay data indicated that **1** was active in a concentration-dependent manner ($EC_{50} = 2.9 \mu M$) but reached a plateau of inhibition of 70% (Figure 1B). Rigorous validation efforts confirmed that the partial inhibition observed was not due to limited solubility (Table S1), compound-induced protein aggregation or off-target mechanisms including RNA binding (Figure S1). In contrast to its behavior in the ATPase assay, **1** showed complete inhibition in the DHX9 unwinding assay ($IC_{50} = 21.4 \mu M$; Figure 1B), further confirming the partial inhibition in the ATPase activity assay was not due to poor compound behavior. To understand further the mechanism of inhibition of the prioritized hit, **1** was tested in a concentration–response ATPase assay using multiple concentrations of either ATP or dsRNA above and below K_M values. The EC_{50} remained within 3-fold of the value under balanced conditions (Figure S2) indicating that **1** is noncompetitive with respect to either substrate. **1** exhibited partial ATPase inhibition irrespective of ATP concentration, lending additional evidence that this behavior was not an artifact related to ATP concentration.

A surface plasmon resonance (SPR) assay¹² was utilized to further confirm binding to apo human DHX9 ($K_D = 0.33 \mu M$). Performing this experiment in the presence of excess ATP did not alter the affinity ($K_D = 0.40 \mu M$). Likewise, the overall compound **1** residence time ($1/k_d$) on DHX9 did not change in the presence or absence of ATP (5.1 vs 5.4 s, respectively;

Figure S3). Taken in total, these experiments show that ATP does not impact the ability of **1** to interact with DHX9, consistent with a noncompetitive mechanism of inhibition for this substrate.

To validate further the binding of **1** to DHX9 and to provide a structural basis for the necessary optimization, structural studies were initiated using the previously disclosed DHX9 crystallography system.¹³ Crystal structures of the DHX9 helicase core from cat and human bound to **1** and ADP were determined (2.27 and 3.26 Å resolution, respectively) and revealed that **1** binds to a pocket at the interface of the RecA1 and MTAD domains (Figure 1C), distal from ADP. The cat and human structures bound to **1** are highly similar in structure (overall rmsd for C_{α} atoms = 0.797 Å) and sequence,¹³ with identical compound binding sites (Figure S4). Unambiguous electron densities were observed in the DHX9 binding pocket for compound **1** and subsequent compounds crystallized with DHX9 (Figure S5). Consistent with the biochemically determined noncompetitive MOI, the binding pocket of **1** is located 20 Å away from the ATP binding site and near the predicted exit site of the ssRNA-binding channel which forms between the lower RecA1/RecA2 domains and the upper OB/HA2 domains. The DHX9 helicase core in complex with **1** adopts the inactive conformation previously reported for DHX9-ADP structures¹³ (rmsd for C_{α} atoms = 0.903 and 0.727 Å, based on superposition of human DHX9 bound to **1** and ADP with PDB ID 8SZP chains A and B, respectively), characterized by a closed ssRNA binding channel and dsRNA-binding domain 2 (dsRBD2) that is dissociated from the helicase core and not visible in the crystal structure.

Compound **1** engages feline DHX9 through a robust network of aromatic, polar and hydrophobic interactions (Figure 1D). Given the overall similarity of the binding pocket across species, this analysis will focus on the higher resolution structure of feline DHX9 bound to **1** unless otherwise noted. The solvent-facing pyrazole ring of **1** is sandwiched between Lys498 and Leu480 of the RecA1 domain and interacts with the side chains of these residues through π -cation and π -hydrogen contacts. Additionally, the side chain of Trp343 from the MTAD domain engages the central benzene ring of **1** via an edge-to-face π - π interaction. **1** is further stabilized in the binding pocket via a robust hydrogen bonding network involving amino acids from the RecA1 and MTAD domains and two water molecules and through van der Waals (VDW) interactions with several hydrophobic residues lining the back and top of the pocket. Structural analysis also shows that this pocket is absent or, if present, not well conserved within the helicase family. The most structurally similar helicase, DHX36, has 42% sequence similarity overall (27% sequence identity) and 50% sequence similarity in the compound **1** binding pocket (22% sequence identity). Consistent with this, **1** shows no inhibition of either DHX36 or the more distantly related helicases SMARCA2 and WRN.⁴ Finally, it was noted that the methyl and ethyl groups on the pyrazole ring extend toward the solvent, providing handles for further optimization.

Optimization of **1 and Identification of Sulfur–Halogen Bond as Driver of Cellular Potency.** With validation of **1** as a reversible binder to and inhibitor of DHX9 and promising preliminary in vitro ADME properties (Table S1), a structurally guided optimization campaign to improve the potency of **1** was initiated. Consistent with the observed binding mode, methylation, removal or replacement of the sulfonamide or amide bonds significantly reduced potency

(Table S2); however, modifications to the pyrazole ring (Table 1) proved more productive.

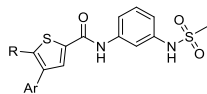
Table 1. Initial Optimization of DHX9 Inhibitor Series^a

Compd	R	ATPase EC ₅₀ (μM)	Unwinding IC ₅₀ (μM)	circBRIP1 EC ₅₀ (μM)
1		4.01	45.3	>30
2		1.56	6.80	>30
3		1.41	1.72	>30
4		0.254	2.26	>30
5		1.28	7.61	---
6		0.708	5.10	>30
7		0.338	4.27	>30
8		0.141	1.40	10.6
9		0.116	1.17	18.3

^aAssay data in all cases derived from 10-point concentration response with a minimum of $n = 2$.

Removal of the ethyl group was tolerated, as seen in compound **2**. This minimal substitution pattern was then used to screen other 5-membered heterocycles, particularly those that could accommodate the nearby/proximal side chains of Ser473 and Ser478 and the backbone carbonyl of Trp343. Although isomeric pyrazole **3** was equipotent to **2**, thiophene **4** was shown to improve potency several fold. Notably, thiophene analogs **4–9** could facilitate coplanarity with the amide carbonyl through a sigma-hole interaction.¹⁴ These compounds continued to show partial ATPase inhibition (58–82% maximum inhibition of ATPase activity) but complete inhibition of unwinding activity, consistent with the behavior of **1**. Introduction of a bromide moiety into compounds **8** or **9** provided the first example of measurable cellular activity in the DHX9 target engagement circBRIP1 induction assay previously described^{4,6} and enabled further optimization of this scaffold via cross-coupling chemistry.

A series of arylated thiophenes were subsequently prepared (Table 2). The seminal analog in this series, phenyl-containing compound **10**, had improvements in ATPase inhibition ($EC_{50} = 0.092 \mu\text{M}$) and unwinding ($IC_{50} = 0.656 \mu\text{M}$) but little effect on cellular circBRIP1 induction. Increasing polarity through various pyridine substitutions (compounds **11–13**) had modestly differing results depending on the placement of the nitrogen atom. In the case of compound **11**, the increase in unwinding inhibition ($IC_{50} = 0.074 \mu\text{M}$) correlated with an associated improvement in circBRIP1 induction ($EC_{50} = 2.11 \mu\text{M}$). Despite this increase in biochemical potency of over 100-

Table 2. Optimization of Arylated Thiophenes^a

Compd	Ar	R	ATPase EC ₅₀ (μM)	Unwinding IC ₅₀ (μM)	circBRIP1 EC ₅₀ (μM)
10		H	0.092	0.656	16.1
11		H	0.020	0.074	2.11
12		H	0.091	0.602	6.32
13		H	0.046	0.788	6.32
14		H	0.054	0.490	5.81
15		H	0.111	0.836	20.7
16		H	0.042	0.643	6.67
17		H	0.099	1.67	12.8
18		H	0.335	1.12	13.4
19		H	0.075	1.21	15.1
20		Me	0.108	1.09	13.2
21		Me	0.004	0.565	1.28
22		Me	0.041	0.440	9.04

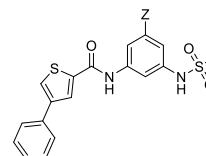
^aAssay data in all cases derived from 10-point concentration response with a minimum of $n = 2$.

fold compared to that of initial hit **1**, circBRIP1 EC₅₀ remained relatively weak. Interestingly, ortho-substitution on the ring was also tolerated for ATPase inhibition (**14**, **15**). Indeed, multiple ortho substituents were additive, with the difluoro compound **16** (ATPase EC₅₀ = 0.042 μM) showing improved potency over the monofluoro compound **15**. Small *meta*-substituent additions such as compounds **17** and **18** broadly maintained ATPase activity (EC₅₀ = 0.099 and 0.335 μM, respectively) but did not improve cellular activity.

Combining findings from the bromo-thiophene **9** and aryl analog **11** led to the identification of methyl-substituted thiophene **21**, which despite a further improvement in ATPase activity (EC₅₀ = 0.004 μM), had only moderate unwinding activity and weak circBRIP1 activity (IC₅₀ = 0.565 and EC₅₀ = 1.28 μM, respectively; Table 2). Interestingly, removal of the pyridine nitrogen to reveal a phenyl ring (compound **22**) resulted in an approximately 10-fold potency reduction in both the ATPase (EC₅₀ = 0.041 μM) and the circBRIP1 (EC₅₀ = 9.04 μM) assays, albeit not in the unwinding assay (IC₅₀ = 0.440 μM). Despite finding nanomolar ATPase inhibitors of DHX9, key SAR features did not directly translate to improved

on-target cellular inhibition of DHX9, as measured by circBRIP1 EC₅₀. To address this, further optimization of the core dianiline structure was explored.

It was noted in the crystal structure of **1** that the thiol side chain of Cys490 was in close proximity to the bound ligand (Figure 1D). This represented an attractive handle for modulating potency, potentially through covalent interactions.¹⁵ Unfortunately, introduction of typical covalent warheads led to significantly diminished potency, and no evidence of covalent attachment was observed crystallographically or biochemically (Table S3).¹⁶ In contrast, the ATPase activity of bromine containing analog **23** (EC₅₀ = 0.156 μM) suggested that small substituents may be tolerated at this position (Table 3). Indeed, methyl-substituted compound **24** also showed

Table 3. Biochemical and Cellular Data of **10**, **23**, and **24**^a

compd	Z	ATPase EC ₅₀ (μM)	Unwinding IC ₅₀ (μM)	circBRIP1 EC ₅₀ (μM)	LS411N IC ₅₀ (μM)	H747 IC ₅₀ (μM)
10	H	0.086	0.643	16.1	>10	>10
23	Br	0.156	0.225	0.765	0.663	>10
24	Me	0.223	1.31	10.9	>10	>10

^aAssay data in all cases derived from 10-point concentration response with a minimum of $n = 2$.

inhibition of ATPase activity. Despite the modest effect on ATPase activity, **23** was also more potent in the helicase unwinding assay (IC₅₀ = 0.225 μM) than either **10** (IC₅₀ = 0.643 μM) or **24** (IC₅₀ = 1.31 μM). More strikingly, **23** showed a substantially differentiated potency in the circBRIP1 assay with a submicromolar EC₅₀ (0.765 μM). Furthermore, this improvement in cellular circRNA induction also demonstrated for the first time a phenotypic consequence, inhibiting MSI-H/dMMR CRC cell line (LS411N) proliferation with an IC₅₀ of 0.663 μM while showing a lack of activity in cells known to be insensitive to DHX9 depletion (NCI-H747, MSS/pMMR CRC), suggesting the antiproliferative behavior is an on-target effect of DHX9 inhibition.⁴ Overall, these results imply a remarkably beneficial contribution of the bromine atom in **23**, leading to a dramatic improvement in cellular functional potency.

To understand further the increased potency of compound **23**, crystal structures of **10** and **23** bound to the helicase core domain of feline DHX9 in the presence of ADP were obtained (2.99 and 2.35 Å resolution, respectively; Figure 2). Both compounds bound to the same DHX9 pocket as **1** utilizing a similar binding mode that maintained the hydrogen bond network of the 1,3-amidosulfonamide core. In addition, the thiophene sulfur of both **10** and **23** was in close proximity to Ser473 and Ser478, suggestive of the sulfur acting as a pseudohydrogen bond donor to the serine hydroxyls, in accordance with the initial design hypothesis. Most notably, a sulfur-halogen bond interaction between the bromine of **23** and the thiol of Cys490 was observed (Figure 2B).

Halogen bonds are of increasing interest in medicinal chemistry, as careful placement of a halogen-bond donor such as an iodine, bromine or chlorine can have substantial impacts

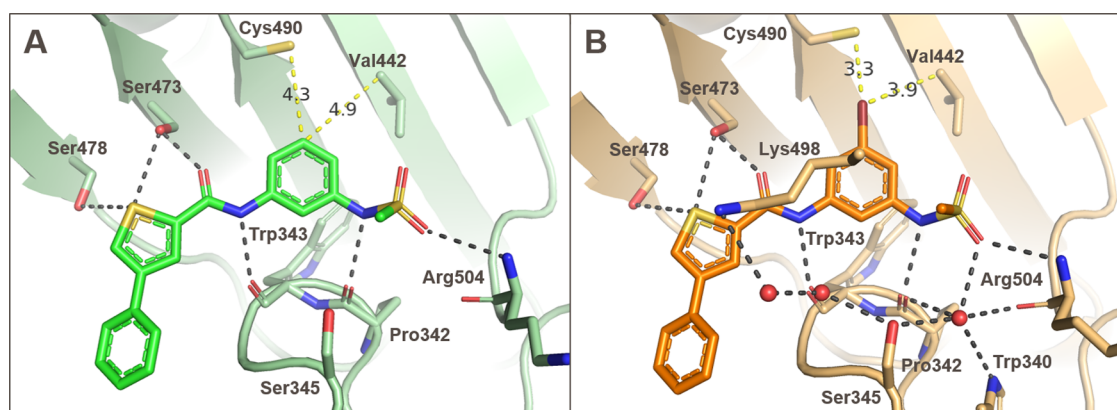


Figure 2. Crystal structures of **10** (PDB 9MFQ) and **23** (PDB 9MFR) bound to feline DHX9 (PDB 8SZQ used as a molecular replacement model for both structures). (A) **10** (green sticks) and (B) **23** (orange sticks) bound to feline DHX9 (cartoon representation). Hydrogen bonds are shown in black dashes, and halogen bonds and VDW interactions are shown in yellow dashes with distances shown in Å.

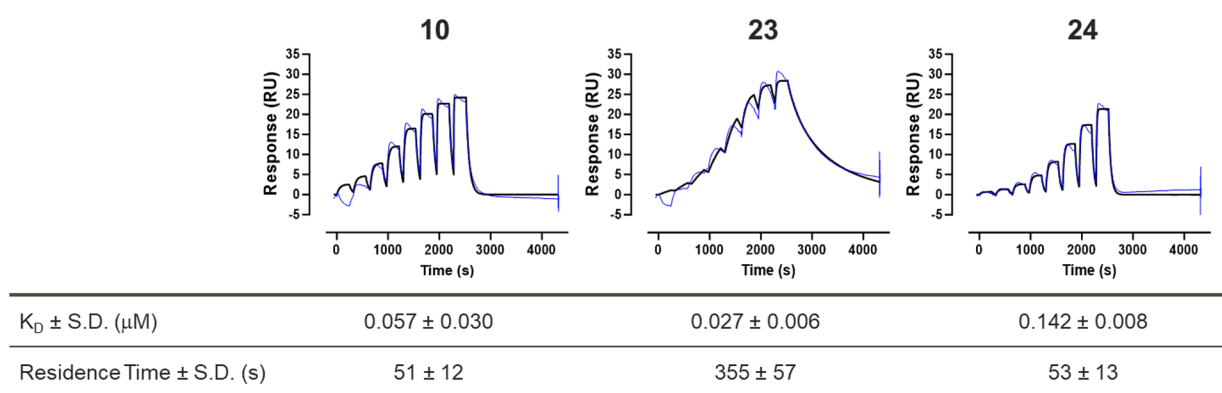


Figure 3. Representative single-cycle SPR sensorgram for **10**, **23**, and **24** binding to DHX9. Experimental data are in blue, mathematically determined best fit to 1:1 binding model (Biacore Insight Evaluation, Cytiva) in black. The off rate of **23** is decreased relative to **10** or **24**, resulting in slower dissociation from the enzyme.

on potency and binding affinity without introducing polar moieties.¹⁷ These interactions tend to be most favorable at distances of around 3.0–3.5 Å and when the orientation is nearly linear, though examples of other orientations are reported.¹⁷ In the case of **23**, the sigma-hole angle between the bromine and the thiol of Cys490 is nearly 180° with a distance of 3.3 Å, suggesting a highly favorable interaction. Additionally, the bromine of **23** reduces the distance to the side chain of Val442 from 4.9 to 3.9 Å, increasing the VDW interaction with that residue. This improved interaction network between DHX9 and compound **23** resulted in an encouraging increase in cellular activity and narrowed the difference between the measured ATPase and unwinding activity (Table 3). To understand better the reason behind these trends, the binding affinity and kinetics of compounds **10**, **23**, and **24** were determined by SPR (Figure 3). Compound **23** appeared to exhibit tighter binding to DHX9 ($K_D = 0.027 \mu\text{M}$) than either **10** or **24** ($K_D = 0.057$ and $0.142 \mu\text{M}$, respectively). Furthermore, stark differences were observed in the off-rates, with compound **23** displaying an approximate 7-fold longer residence time in SPR than either **10** or **24** (355 versus 51 and 53 s, respectively). Binding of **23** was also shown to stabilize the DHX9-RNA substrate complex by an additional 1.1–1.4 °C compared to **10** in a thermal shift assay (Figure S6 and Table S4). In contrast, **24** affords no additional stabilization relative to **10** in this assay.

Compound **1** and other compounds from this series (vide supra) are noncompetitive with respect to both ATP and RNA, suggesting that binding kinetics derived from SPR (run in the absence of RNA) should not be impacted.¹⁸ To understand better the key drivers of functional DHX9 inhibition, correlations between the ATPase, circBRIP1 and SPR assays were interrogated (Figure 4). First, it was noted that the maximal inhibition observed in the ATPase or unwinding assay was independent of potency (Figure 4A), suggesting that the mechanism of inhibition was likely consistent regardless of compound potency. Meanwhile, there is a moderate correlation between ATPase activity and circBRIP1 elevation ($R^2 = 0.49$, Figure 4B). More specifically, multiple compounds with almost identical potencies in the ATPase assay have widely different circBRIP1 EC_{50} values, suggesting some disconnect despite an overall correlation trend. A subset of compounds was then analyzed via SPR to understand binding affinity and kinetics. As seen in Figure 4C, a general relationship between binding affinity (K_D) and circBRIP1 potency (EC_{50}) is observed, but some outliers remain, and the correlation was not markedly improved ($R^2 = 0.55$). In contrast, a clear correlation emerged ($R^2 = 0.84$, $P < 0.01$) between circBRIP1 EC_{50} and SPR residence time, suggesting that this parameter is a key contributor to improved cell potency (Figure 4D). Notably, all compounds with residence time >1000 s contain a halogen atom pointed toward Cys490. Further, a strong correlation between circBRIP1 EC_{50} and

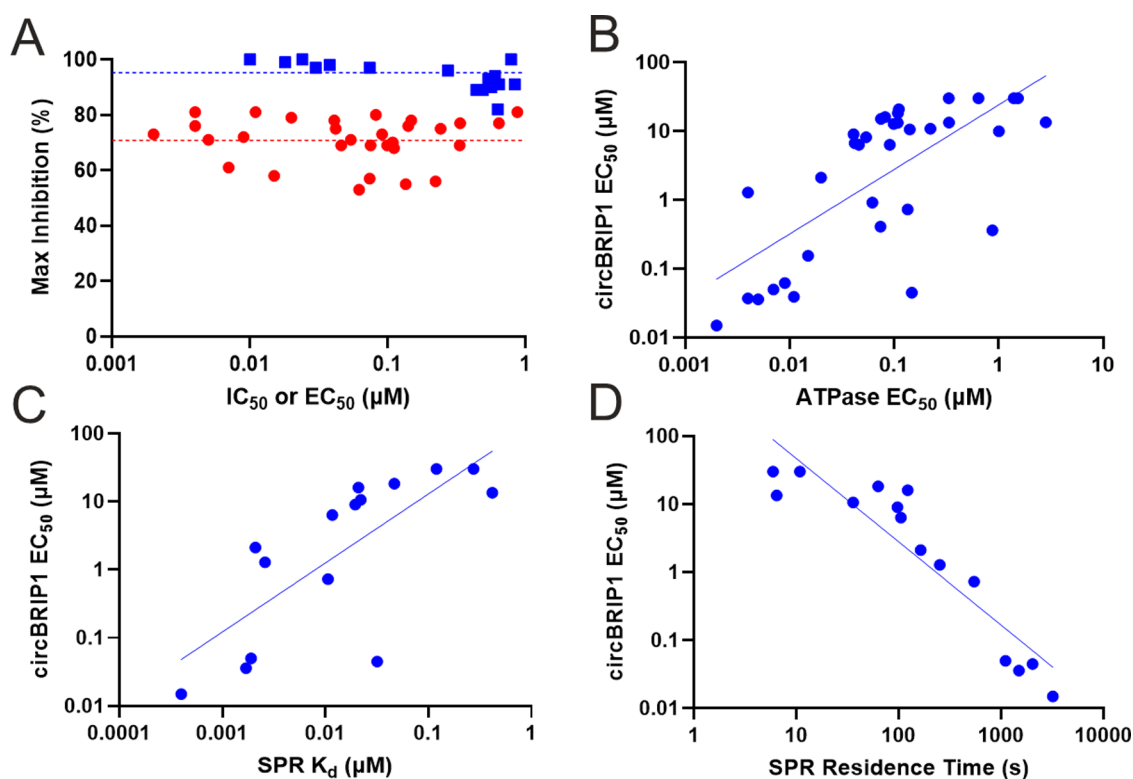


Figure 4. Biochemical, biophysical, and cellular correlations of DHX9 inhibitors. (A) Maximum inhibition (%) vs EC_{50} (ATPase assay, red) or IC_{50} (unwinding assay, blue). Dashed line is the mean value (ATPase assay: 70.3%; unwinding assay: 95.3%). (B) circBRIP1 EC_{50} vs ATPase EC_{50} . Line of best fit drawn ($R^2 = 0.49$). (C) circBRIP1 EC_{50} vs K_D . Line of best fit drawn ($R^2 = 0.55$). (D) circBRIP1 EC_{50} vs SPR residence time. Line of best fit drawn ($R^2 = 0.84$).

LS411N antiproliferative IC_{50} is also observed (Figure S7). In summary, the interaction with the Cys490 thiol appears to be responsible for the longer residence time of the series irrespective of affinity, ultimately leading to improved functional inhibition of DHX9 and driving further optimization.

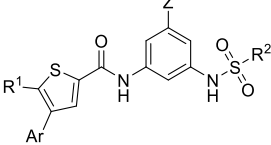
Compound **23** was further profiled (Table S1). Of note is the relatively low solubility ($10.6 \mu\text{M}$) in fasted state simulated intestinal fluid (FaSSIF) media, potentially due to its high degree of unsaturation and lipophilicity ($c\text{LogP} = 3.77$). The pharmacokinetic (PK) profile determined in CD1 mice showed a high unbound clearance of $22,400 \text{ mL}/\text{min}/\text{kg}$ and a modest unbound C_{max} of 3.1 nM and $\text{AUC}_{0-24\text{h}}$ of $6.4 \text{ h}\cdot\text{nM}$. To test the hypothesis that in vivo inhibition would result in robust tumor growth inhibition, the focus moved to improving potency, solubility and PK properties to deliver a suitable in vivo tool compound.

Optimization to Tool Compound ATX968. Given the improved cellular potency of **23** in the circBRIP1 assay, inclusion of this key halogen-sulfur bond was deemed critical in our pursuit of a suitable tool compound. Thus, optimization was undertaken to identify a halogen-containing compound with suitable cellular potency to act as a tool for demonstrating the effects of inhibiting DHX9 in vitro and in vivo (Table 4). Building on earlier SAR understandings, modification of the phenyl ring of **23** to a pyridine afforded **25**, resulting in improvement in potency across all activity assays and in solubility. Aiming to reduce molecular weight and lipophilicity, bromine was further replaced with a chlorine, resulting in compound **26** which had modest improvement in solubility and no appreciable change in cellular activity (circBRIP1 $EC_{50} = 0.062$ and LS411N $IC_{50} = 0.253 \mu\text{M}$). Additional tactics to

improve solubility included disruption of planarity through installation of small groups at the periphery of the molecule.¹⁹

A survey of various substituents on the phenyl ring *ortho* to the thiophene led to greatly improved solubility as seen in **27** (FaSSIF sol. = $160 \mu\text{M}$) and **28** (FaSSIF sol. = $165 \mu\text{M}$), though these were weaker against circBRIP1 ($EC_{50} = 160$ and $0.913 \mu\text{M}$, respectively). Once again leveraging prior SAR data, insertion of a methyl group onto the thiophene ring (compound **29**) facilitated further improvement of the circBRIP1 EC_{50} ($0.015 \mu\text{M}$), albeit with diminished solubility (FaSSIF sol. = $16.1 \mu\text{M}$). Further elaboration around the pyridine ring and the alkyl sulfonamide of **29** provided mixed results as exemplified by compounds **30–32**, with an inverse relationship emerging between cellular potency and solubility. For example, **30** retained moderate antiproliferative activity but significantly reduced solubility, whereas **31** had improved solubility but showed no improvement in proliferation IC_{50} activity compared to **29**. Other attempts to increase three-dimensional character, such as ethyl sulfonamide **32**, were also not successful due to decreased cellular potency (circBRIP1 $EC_{50} = 0.154$ and LS411N $IC_{50} = 0.321 \mu\text{M}$).

ATX968 was identified as a potential tool compound, as it demonstrated a desirable balance between on-target antiproliferative inhibition activity (LS411N $IC_{50} = 0.069$; H747 $IC_{50} > 10 \mu\text{M}$) and solubility (FaSSIF sol. = $62.5 \mu\text{M}$; simulated gastric fluid sol. = $264 \mu\text{M}$). Consistent with the uniqueness of the binding site, broader biochemical profiling of **ATX968** illustrated excellent selectivity against other related helicases (DHX36, SMARCA2 and WRN) and kinases (a panel of 97 diverse kinases).⁴

Table 4. Optimization of Halogen-Containing Compounds^a


Compd	Ar	Z	R ¹	R ²	ATPase EC ₅₀ (μM)	circBRIP1 EC ₅₀ (μM)	LS411N IC ₅₀ (μM)	FaSSiF solubility (μM)
23		Br	H	Me	0.156	0.765	0.663	136
25		Br	H	Me	0.002	0.052	0.275	20.4
26		Cl	H	Me	0.009	0.062	0.253	29.4
27		Cl	H	Me	0.074	0.410	---	160
28		Cl	H	Me	0.062	0.913	---	165
29		Cl	Me	Me	0.002	0.015	0.117	16.1
30		Cl	Me	Me	0.130	0.045	0.132	3.7
31		Cl	Me	Me	0.011	0.039	0.119	152
32		Cl	H	Et	0.015	0.154	0.321	102
ATX968		Cl	H	Me	0.003	0.060	0.069	62.5

^aAssay data (except for FaSSiF solubility) derived from 10-point concentration response with a minimum of $n = 2$.

The co-complex crystal structure with ATX968 was determined using feline DHX9 (2.43 Å resolution, Figure 5A). The same binding mode as 23 was observed, with all major interactions preserved including the key halogen–sulfur bond. Halide exchange from bromine to chlorine in ATX968 was well-tolerated with no perceptible effect on the halogen–sulfur interaction. The ATX968 pyridine nitrogen formed a

water-mediated hydrogen bond to the Lys498 side chain, providing an additional anchoring point to the robust hydrogen bond network that may contribute to the increased potency of ATX968. Torsion profile analysis suggested that free ligand geometry may also contribute to potency gain, as the methylpyridyl moiety may be able to preorganize into the bioactive conformation prior to DHX9 binding. One of the ATX968 local energy minima occurred at a dihedral angle of $\sim 35^\circ$ between the thiophene and pyridyl rings, which corresponds to the bioactive conformation observed for both ATX968 and 23. To enable comparison between the cat and human proteins bound to the tool compound, a crystal structure of ATX968 bound to human DHX9 was determined (2.75 Å resolution, Figure 5B). As expected, overlay of the ligand-bound structures showed a high degree of overlap, verifying that the higher resolution feline DHX9 structures were excellent surrogates for human DHX9 (overall and binding pocket rmsd for C_α atoms = 0.605 and 0.144 Å, respectively).

To determine its suitability as an in vivo tool compound, ATX968 was profiled in a battery of ADME/PK assays (Table S1). In addition to its favorable solubility, ATX968 had favorable permeability in a Caco-2 assay (A → B rate of 7.68×10^{-6} cm/s; efflux ratio of 3.5). Mouse PK profiling highlights a significant improvement in unbound clearance (3661 mL/min/kg) and a higher unbound exposure (AUC_{0–24h,u} = 39.6 h·nM; C_{max,u} = 19.9 nM) when compared to compound 23. Intrinsic unbound clearance in mouse hepatocytes was observed to be 1250 mL/min/kg, within 3-fold of the observed unbound plasma clearance in CD1 mice. To identify a suitable dose for studying in vivo effects of DHX9 inhibition, dose-escalation studies in Balb/C mice (the intended mouse strain for tumor xenograft models) were initiated (Figure 6A and Table S5). Based on preliminary in vivo target engagement studies, exposure concentrations capable of covering the protein binding corrected circBRIP1 EC₉₀ for 24 h were desired. Accordingly, a target C_{min} concentration was identified as 3964 ng/mL. Dose escalations through 10, 100, and 300 mg/kg in Balb/C mice displayed a dose proportional increase in C_{max} and a greater than proportional increase in AUC with a concomitant increase in oral half-life ($t_{1/2}$) from 1.42 to 14.7 h (Table S5). The ratio of the C_{max} to the dose remains consistent, but the dose-normalized AUC_{0–24h} increases with increasing dose (Figure 6B). This may be due to saturation of clearance mechanisms and hepatic recirculation, among other

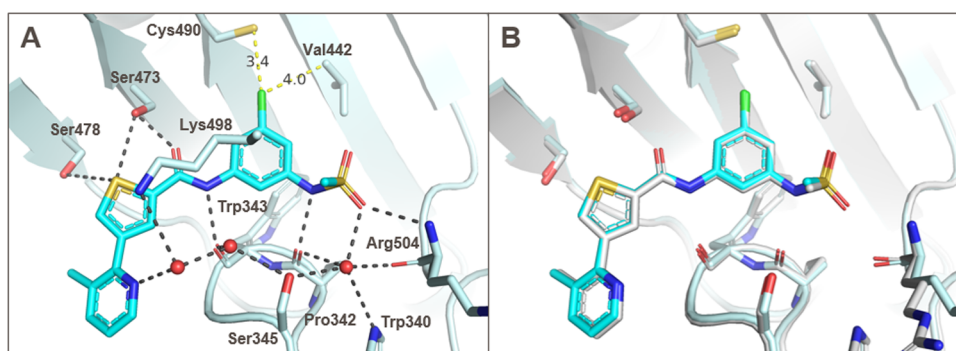


Figure 5. Crystal structures of ATX968 bound to cat and human DHX9 proteins. A) Crystal structure of ATX968 (cyan sticks) complexed with ADP-bound feline DHX9 (PDB 9MFS; PDB 8SZQ used as a molecular replacement model). Coordinated waters shown as red spheres. B) Structure from A superposed with the human DHX9-ADP-ATX968 complex (gray) (PDB 9MFT; PDB 8SZP used as a molecular replacement model).

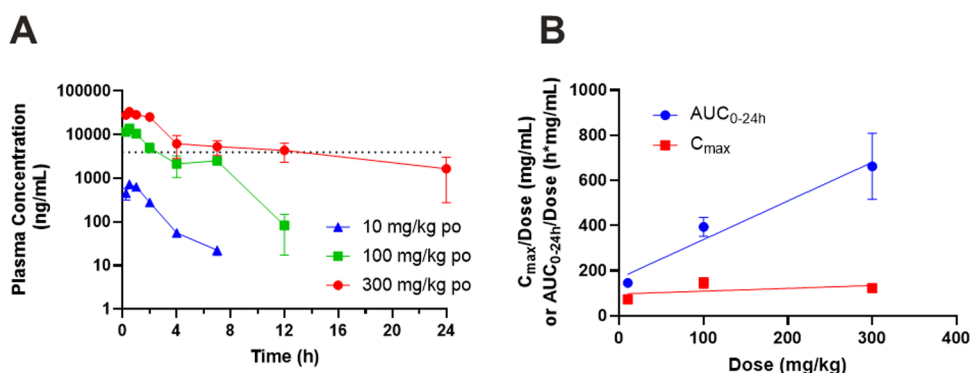


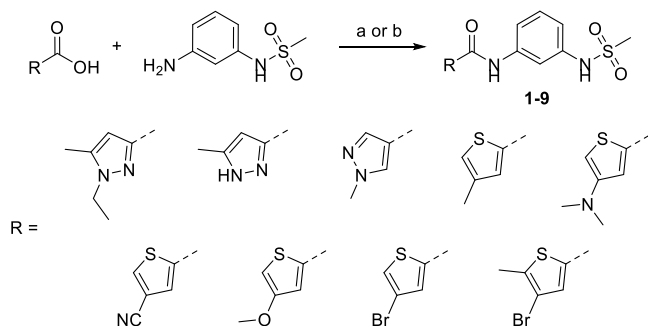
Figure 6. Pharmacokinetics of ATX968 at escalating doses in mice. (A) Pharmacokinetic profile of a single oral dose of ATX968 in CD1 mice (10 mg/kg, blue triangles) and Balb/C mice (100 mg/kg, green squares and 300 mg/kg, red circles). The dotted line is the plasma-protein binding corrected circBRIP1 EC₉₀. (B) Plot of dose-normalized C_{max} (red squares) and AUC_{0-24h} (blue circles) of ATX968. Line of best fit drawn separately for each end point.

factors. Flip-flop kinetics cannot be ruled out based on the properties of ATX968 trending toward a BDDCS class 3 or 4 characterization.²⁰ The 300 mg/kg dose was able to exceed the target C_{min} exposure for 24 h with twice daily dosing (C_{min} = 5870 ng/mL) and determined to be suitable for a tool compound to enable *in vivo* proof of concept studies. As previously reported, ATX968 was well tolerated at doses of 300 mg/kg b.i.d. po over a period of 28 days and resulted in durable tumor regression in dMMR/MSI-H CRC xenograft models.⁴

CHEMICAL OPTIMIZATION

As part of confirmation of potency, compound **1** was synthesized as described in Scheme 1. This route enabled

Scheme 1. Synthesis of Compounds 1–9^a



^aReagents and conditions: (a) TCFH, NMI, MeCN, rt. (b) HATU, DIPEA, DMF, rt.

rapid exploration of other structures outlined in Table 1 (vide supra), using either HATU or TCFH to affect an amide coupling, typically from commercially available materials.

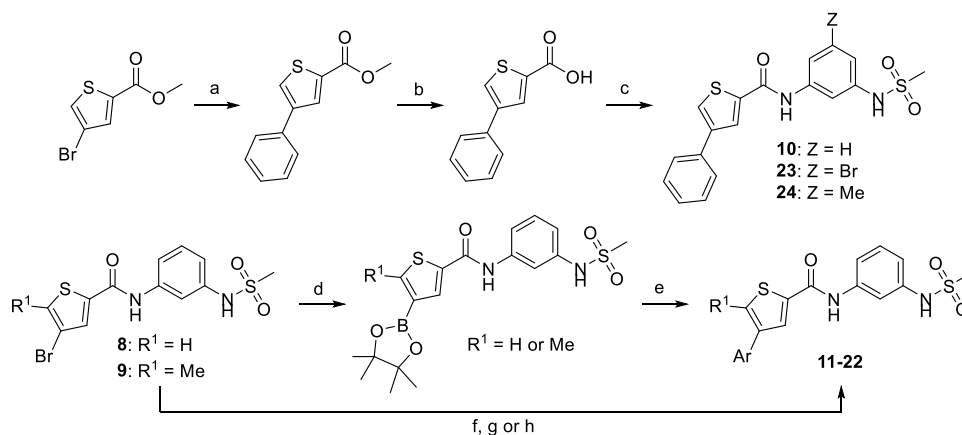
As more diverse substituents were appended to the thiophene ring, a more modular synthesis was sought to expedite analog generation, as outlined by the approaches shown in Scheme 2. To prepare compounds **10**, **23**, and **24**, a Suzuki cross-coupling of methyl 4-bromothiophene-2-carboxylate with phenylboronic acid provides an intermediate ester, which after acid hydrolysis and TCFH-mediated amide coupling with an appropriate aniline gave target compounds **10**, **23**, and **24**. Synthesis of additional analogs were performed through one of two methods. The first method involved borylation of the thiophene, followed by coupling of an

appropriate aryl halide, such as 2-bromopyridine to provide **11** or 2-bromo-4-methoxy-1-methylbenzene to yield **20**. Alternatively, additional analogs that vary the solvent-exposed aryl group were obtained through a more direct route, starting from halides **8** or **9** and directly arylated via Suzuki or Stille couplings.

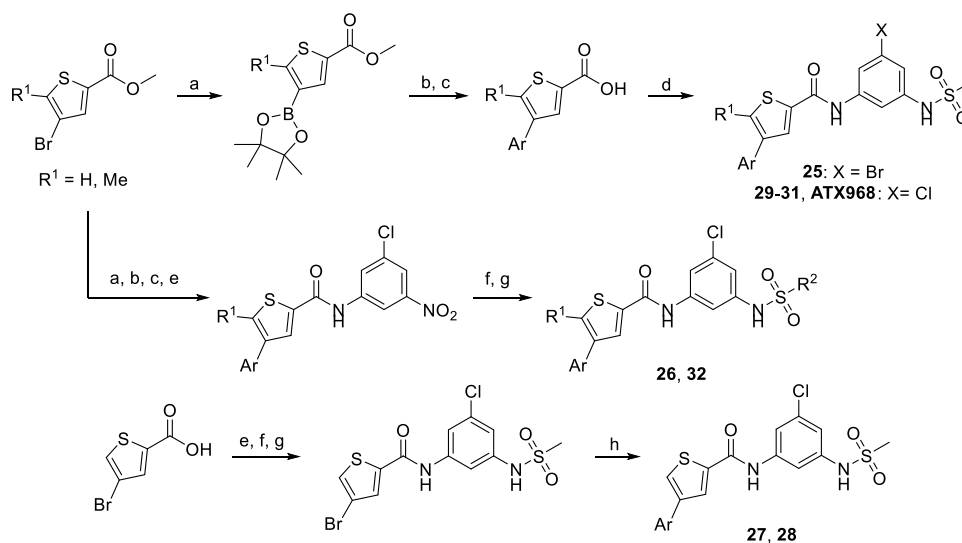
Scheme 3 shows the approaches used to synthesize the remaining compounds from Table 4. Compounds **25**, **29–31**, and ATX968 were built in a similar manner to compounds **10**, **23**, and **24** namely, by elaboration of thiophene methyl ester via borylation, Suzuki coupling, ester hydrolysis and TCFI mediated coupling with the desired halogenated aniline. This approach was also scalable, ultimately delivering over 100 g of ATX968. Compounds **26** and **32** followed a similar procedure except for the final coupling step. With these exemplars, the thiophene intermediate was coupled with 3-chloro-5-nitroaniline, with the products subjected to hydrogenation of the nitro-group and final sulfonamide formation yielding the final compounds. Lastly, analogs **27** and **28** utilized 4-bromothiophene-2-carboxylate for amide coupling with 3-chloro-5-nitroaniline. This was followed again by iron-mediated hydrogenation and subsequent sulfonamide formation using the aniline and methane sulfonyl chloride. The resulting bromo-thiophene intermediates were coupled with 2-(2,6-difluorophenyl)-4,4,5,5-tetramethyl-1,3,2-dioxaborolane or (2-methoxyphenyl) boronic acid under suitable conditions to produce targets **27** and **28**, respectively. Taken together, the various routes presented here demonstrate the ability to modulate each moiety of the compound class, enabling interrogation of diverse structure–activity relationships ultimately culminating in the identification of ATX968.

DISCUSSION AND CONCLUSIONS

The work presented herein covers the discovery and optimization of the first inhibitors of the RNA helicase DHX9, an important and novel target in oncology. Helicases are structurally complex, characterized by the presence of multiple core and regulatory domains that undergo conformational rearrangements during the catalytic cycle and have been historically difficult targets for drug discovery.^{21,22} Despite these challenges, significant progress has been recently made in finding potent and selective small molecule inhibitors for members of this target class, including Bloom syndrome protein BLM, DDX3 and SMARCA2.^{23–26} In addition to inhibitory approaches, targeted protein degradation has also

Scheme 2. Synthesis of Arylated Thiophenes^a

^aReagents and conditions: (a) PhB(OH)₂, Pd(dppf)Cl₂, K₃PO₄, 1,4-dioxane, water, 80 °C. (b) LiOH, THF, water, rt. (c) TCFH, NMI, *N*-(3-anilino)methanesulfonamide, MeCN, rt. (d) B₂pin₂, Pd(dppf)Cl₂, KOAc, 1,4-dioxane, 80 °C. (e) ArBr, Pd(dppf)Cl₂, K₂CO₃, 1,4-dioxane, water, 80 °C. (f) ArB(OH)₂, Pd(PPh₃)₂Cl₂, Na₂CO₃, EtOH, water, 80 °C. (g) ArB(OH)₂, K₂CO₃, Pd(dppf)Cl₂, 1,4-dioxane, water, 80 °C. (h) ArSn(Bu)₃, Pd(PPh₃)₄, toluene, 120 °C.

Scheme 3. Synthesis of ATX968 and Analogs^a

^aReagents and conditions: (a) B₂pin₂, Pd(dppf)Cl₂, potassium acetate, 1,4-dioxane, 80 °C. (b) ArBr, Pd(dppf)Cl₂, K₂CO₃, 1,4-dioxane, water, 90 °C or Pd(PPh₃)Cl₂, Na₂CO₃, EtOH, water, 80 °C. (c) LiOH, EtOH, or MeOH, H₂O, rt. (d) *N*-(3-Amino-5-chlorophenyl)methanesulfonamide, TCFH, NMI, MeCN, rt. (e) 3-chloro-5-nitroaniline, TCFH, NMI, MeCN. (f) Fe, NH₄Cl, MeOH, H₂O. (g) R₂SO₂Cl, pyridine, rt. (h) 2-(2,6-Difluorophenyl)-4,4,5,5-tetramethyl-1,3,2-dioxaborolane, XPhosPdG3, K₃PO₄, 1,4-dioxane, 80 °C or (2-methoxyphenyl)boronic acid, Pd(dppf)Cl₂, K₂CO₃, 1,4-dioxane, 80 °C.

been explored, particularly against SMARCA2/4.²⁷ Most notably, multiple covalent^{28–30} and noncovalent³¹ inhibitors of Werner syndrome protein WRN have also been identified, leading to compounds currently in clinical development.³²

Owing to its unexpected partial inhibition of ATPase activity, the allosteric hit **1** may have been overlooked in a typical high-throughput screening triage if a dogmatic approach to identifying dead-end inhibitors capable of completely abrogating ATPase activity was followed.³³ Alternatively, a reliance only on ATPase activity for validation of chemical matter could easily have caused compound **1** to be deprioritized if the low plateau observed was attributed to lower concentrations of compound **1** in assay. A rigorous analysis of the biochemical and biophysical data associated with **1** and coupled with a high-quality crystal structure with

DHX9 to elucidate the binding site allowed full validation of **1** as a genuine inhibitor of DHX9. This early investment in the target enabled a successful optimization campaign, ultimately delivering a tool compound suitable for in vivo interrogation of DHX9 and proof of concept as a viable drug target. Notably, all potent derivatives of **1**, including ATX968, show similar degrees of ATPase inhibition at saturating concentrations, suggesting that this partial inhibition is a consistent feature of this series using available assays (Figures 4A and S8). This behavior was not observed with ATP-competitive inhibitor GTPγS, which displayed full inhibition of the ATPase assay at saturating concentrations, and was functionally distinct from previously reported helicase inhibitors.^{12,23–32} The exact mechanism of ATP hydrolysis and unwinding activity in the helicase cycle of DHX9 and its closely related *Drosophila*

homologue MLE is an active area of investigation.³⁴ Additional studies to probe the mechanics of ATX968 inhibition of DHX9 enzymatic activity will be required.

In the process of optimization, the discovery of the sulfur-halogen interaction between the thiol of Cys490 and the bromine of **23** was critical to identifying a path forward for this series. This interaction, which does not substantially alter binding affinity or inhibition of ATPase activity, appears to be responsible for the longer residence time of **23**, ultimately leading to improved cellular potency. Although the differences in residence time are relatively modest, a molecular motor such as DHX9 that likely proceeds through a processive reaction mechanism may be more sensitive to inhibitor off-rates.³⁵ In addition, residence time has been shown to correlate particularly well to cellular or in vivo potency, due to a prolonged duration of action leading to a stronger (i.e., longer-lived) pharmacodynamic effect.^{36–38}

ATX968 was identified as a novel tool compound suitable for in vitro and in vivo studies which enables further exploration of the biology of DHX9. From a diversity library screening hit with only partial inhibition of the target enzyme, the series was expanded and optimized, uncovering a unique and specific binding site. Using SBDD, a key halogen-bond was identified which facilitated a significant improvement in cellular activity, demonstrating a high degree of target engagement, on target antiproliferative activity and in vivo tumor growth inhibition, ultimately validating DHX9 as a potential novel cancer target.⁴

EXPERIMENTAL SECTION

General Synthetic Methods. Unless otherwise noted, all chemical reagents and reaction solvents were purchased from commercial suppliers and used as received. Air or moisture sensitive reactions were carried out under a nitrogen or argon atmosphere. Normal phase column chromatography was performed using silica gel as the stationary phase. Reverse phase column chromatography was performed on C18 silica gel columns, using either an acidic (MeCN/water with 0.1% formic acid) or basic (MeCN/water with 10 mM NH₄HCO₃), unless otherwise noted. Proton nuclear magnetic resonance (¹H NMR) spectra were recorded at 300 or 400 MHz on a Bruker AVANCE spectrometer. For ¹H NMR spectra, chemical shifts are reported in ppm and are reported relative to residual nondeuterated solvent signals. The following abbreviations (or a combination, thereof) are used to describe splitting patterns: s, singlet; d, doublet; t, triplet; q, quartet; m, multiplet; br, broad. Coupling constants are reported in Hz. Carbon magnetic resonance spectra (¹³C NMR) were recorded at 75 or 100 MHz on a Bruker AVANCE spectrometer. All compounds are >95% pure by HPLC or LC-MS (UHPLC) analysis. LC-MS system used consisted of either a Shimadzu-2020 LC-MS platform with electrospray ionization in positive ion detection mode (Column: Halo 30 mm; Mobile Phase A: water/0.1% formic acid in water; Mobile Phase B: MeCN/0.1% formic acid in water; Flow rate 1.5 mL/min; Gradient 5–70% B in 2 min then 70–100% B) (Condition A), Shimadzu-2020 LC-MS platform with electrospray ionization in positive ion detection mode (Column: Kinetex EVO C18, 3.0 × 50 mm, 2.6 μm; Mobile Phase A: water/5 mM NH₄HCO₃; Mobile Phase B: MeCN; Flow rate 1.2 mL/min; Gradient 10–70% B) or Agilent Technologies 1290 series (Binary Pump, Diode Array Detector, Column: Agilent Poroshell 120 EC-C18, 2.7 μm, 4.6 × 50 mm column. Mobile phase: A: 0.05% formate in water (v/v), B: 0.05% formate in MeCN (v/v). Flow Rate: 1 mL/min at 25 °C). HRMS system used consisted of Agilent LC-TOF with an Agilent SB-C18 (50 × 2.1 mm, 1.8 μm) column.

Synthesis of 1-Ethyl-N-(3-methanesulfonamidophenyl)-5-methylpyrazole-3-carboxamide (1). To a stirred solution of 1-ethyl-5-methylpyrazole-3-carboxylic acid (500 mg, 3.2 mmol) in MeCN (10

mL) was added *N*-(3-aminophenyl)methanesulfonamide (724.7 mg, 3.9 mmol, 1.2 equiv), NMI (798.8 mg, 9.72 mmol, 3 equiv) and TCFH (1364.9 mg, 4.8 mmol, 1.5 equiv). The resulting mixture was stirred for 1 h at rt. The resulting mixture was concentrated under vacuum. The residue was purified by reverse phase column chromatography to afford 1-ethyl-*N*-(3-methanesulfonamidophenyl)-5-methylpyrazole-3-carboxamide (**1**, 260.2 mg, 0.807 mmol, 25% yield) as a white solid. ¹H NMR (400 MHz, DMSO-*d*₆) δ 9.89 (s, 1H), 9.74 (s, 1H), 7.75 (t, *J* = 2.1 Hz, 1H), 7.53 (dd, *J* = 8.1, 2.0 Hz, 1H), 7.25 (t, *J* = 8.1 Hz, 1H), 6.92–6.85 (m, 1H), 6.55 (s, 1H), 4.16 (q, *J* = 7.2 Hz, 2H), 3.02 (s, 3H), 2.32 (s, 3H), 1.37 (t, *J* = 7.2 Hz, 3H). ¹³C NMR (DMSO-*d*₆) δ 160.7, 145.3, 140.3, 140.1, 139.1, 129.7, 116.1, 115.3, 112.0, 106.7, 44.5, 15.6, 11.0. LC-MS Purity 99.7%. HRMS (ESI+) 323.1185.

Synthesis of *N*-(3-Methanesulfonamidophenyl)-5-methyl-1H-pyrazole-3-carboxamide (2). A mixture of 5-methyl-1H-pyrazole-3-carboxylic acid (100 mg, 0.79 mmol), HATU (448 mg, 1.18 mmol, 1.5 equiv) and ethylbis(propan-2-yl)amine (306 mg, 2.37 mmol, 3 equiv) in DMF (3 mL) was stirred at rt for 10 min. *N*-(3-Aminophenyl)methanesulfonamide (147 mg, 792 μmol) was added and the reaction was stirred at rt for 2 h. The mixture was diluted with water (10 mL), then extracted with EtOAc (3 × 20 mL). The combined organic extracts were washed with water (3 × 10 mL) and brine (10 mL), dried over sodium sulfate and concentrated in vacuo. The residue was purified by preparative TLC to afford *N*-(3-methanesulfonamidophenyl)-5-methyl-1H-pyrazole-3-carboxamide (**2**, 60.0 mg, 0.204 mmol, 26% yield) as a light yellow solid. ¹H NMR (400 MHz, methanol-*d*₄) δ 7.74 (t, *J* = 2.1 Hz, 1H), 7.43 (ddd, *J* = 8.1, 2.1, 1.0 Hz, 1H), 7.30 (t, *J* = 8.1 Hz, 1H), 7.02 (ddd, *J* = 8.1, 2.3, 1.0 Hz, 1H), 6.58 (s, 1H), 3.00 (s, 3H), 2.35 (s, 3H). HPLC Purity 99%. LC-MS (ESI+) 295.15.

Synthesis of *N*-(3-Methanesulfonamidophenyl)-1-methyl-1H-pyrazole-4-carboxamide (3). Following the procedure for **2**, purification by reverse phase preparative HPLC provided *N*-(3-methanesulfonamidophenyl)-1-methyl-1H-pyrazole-4-carboxamide (**3**, 20.0 mg, 0.0680 mmol, 25% yield) as a white solid. ¹H NMR (400 MHz, DMSO-*d*₆) δ 9.85 (s, 1H), 9.75 (s, 1H), 8.31 (s, 1H), 8.01 (d, *J* = 0.7 Hz, 1H), 7.64 (t, *J* = 2.1 Hz, 1H), 7.53–7.44 (m, 1H), 7.26 (t, *J* = 8.1 Hz, 1H), 6.89 (ddd, *J* = 8.1, 2.2, 1.0 Hz, 1H), 3.89 (s, 3H), 2.99 (s, 3H). ¹³C NMR (75 MHz, DMF-*d*₇) δ 161.2, 141.0, 139.5, 139.1, 132.8, 129.6, 119.3, 115.7, 115.0, 111.6, 38.9. HPLC purity 99%. LC-MS (ESI+) 295.15.

Synthesis of *N*-(3-Methanesulfonamidophenyl)-4-methylthiophene-2-carboxamide (4). Following the procedure for **1**, purification by reverse phase column chromatography (5–95% MeCN/H₂O, acidic conditions) provided *N*-(3-methanesulfonamidophenyl)-4-methylthiophene-2-carboxamide (**4**, 46.4 mg, 0.149 mmol, 21% yield) as a white solid. ¹H NMR (300 MHz, DMSO-*d*₆) δ 10.22 (s, 1H), 9.79 (s, 1H), 7.87 (d, *J* = 1.4 Hz, 1H), 7.67 (t, *J* = 2.1 Hz, 1H), 7.55–7.42 (m, 2H), 7.29 (t, *J* = 8.1 Hz, 1H), 6.97–6.88 (m, 1H), 3.01 (s, 3H), 2.28 (d, *J* = 1.0 Hz, 3H). ¹³C NMR (101 MHz, DMF-*d*₇) δ 160.59, 140.54, 140.25, 139.62, 138.66, 131.17, 129.69, 127.43, 115.91, 115.35, 111.85, 38.90, 15.20. LC-MS Purity 98.7%. LC-MS (ESI+) 311.05.

Synthesis of 4-(Dimethylamino)-*N*-(3-methanesulfonamidophenyl)thiophene-2-carboxamide (5). Following the procedure for **1**, purification by reverse phase column chromatography (5–95% MeCN/H₂O, acidic conditions) provided 4-(dimethylamino)-*N*-(3-methanesulfonamidophenyl)thiophene-2-carboxamide (**5**, 31.4 mg, 0.0925 mmol, 30% yield) as a white solid. ¹H NMR (400 MHz, DMSO-*d*₆) δ 10.14 (s, 1H), 9.79 (s, 1H), 7.80 (d, *J* = 1.7 Hz, 1H), 7.65 (t, *J* = 2.1 Hz, 1H), 7.51–7.44 (m, 1H), 7.29 (t, *J* = 8.1 Hz, 1H), 6.97–6.89 (m, 1H), 6.46 (d, *J* = 1.7 Hz, 1H), 3.00 (s, 3H), 2.82 (s, 6H). ¹³C NMR (101 MHz, DMF-*d*₇) δ 160.52, 153.15, 140.37, 139.46, 138.88, 129.53, 120.64, 115.70, 115.15, 111.62, 103.12, 41.42, 38.72. LC-MS purity 99.2%. LC-MS (ESI+) 340.10.

Synthesis of 4-Cyano-*N*-(3-methanesulfonamidophenyl)thiophene-2-carboxamide (6). Following the procedure for **2**, purification by reverse phase column chromatography (5–95%

MeCN/H₂O, acidic conditions) provided 4-cyano-*N*-(3-methanesulfonamidophenyl)thiophene-2-carboxamide (**6**, 31.2 mg, 0.0971 mmol, 18% yield) as a white solid. ¹H NMR (400 MHz, methanol-*d*₄) δ 8.48 (d, *J* = 1.2 Hz, 1H), 8.13 (d, *J* = 1.3 Hz, 1H), 7.73 (t, *J* = 2.1 Hz, 1H), 7.42 (ddd, *J* = 8.1, 2.0, 1.0 Hz, 1H), 7.32 (t, *J* = 8.1 Hz, 1H), 7.04 (ddd, *J* = 8.0, 2.2, 1.0 Hz, 1H), 2.99 (s, 3H). ¹³C NMR (101 MHz, DMF-*d*₇) δ 159.12, 143.13, 141.94, 140.01, 139.76, 139.70, 130.30, 129.77, 116.07, 115.84, 114.91, 111.98, 110.57, 38.96. LC-MS Purity 97.3%. LC-MS (ESI+) 322.00.

Synthesis of *N*-(3-Methanesulfonamidophenyl)-4-methoxythiophene-2-carboxamide (7). Following the procedure for **1**, purification by reverse phase column chromatography (5–95% MeCN/H₂O, acidic conditions) provided *N*-(3-methanesulfonamidophenyl)-4-methoxythiophene-2-carboxamide (**7**, 6.2 mg, 0.0190 mmol, 6% yield) as a white solid. ¹H NMR (400 MHz, DMSO-*d*₆) δ 10.21 (s, 1H), 9.79 (s, 1H), 7.75 (d, *J* = 1.7 Hz, 1H), 7.65 (t, *J* = 2.1 Hz, 1H), 7.48 (ddd, *J* = 8.2, 2.1, 1.0 Hz, 1H), 7.29 (t, *J* = 8.1 Hz, 1H), 6.98–6.90 (m, 2H), 3.79 (s, 3H), 3.00 (s, 3H). LC-MS Purity 98.3%. LC-MS (ESI+) 327.05.

Synthesis of 4-Bromo-*N*-(3-methanesulfonamidophenyl)thiophene-2-carboxamide (8). Following the procedure for **2**, purification by preparative HPLC provided 4-bromo-*N*-(3-methanesulfonamidophenyl)thiophene-2-carboxamide (**8**, 31.2 mg, 0.0831 mmol, 56% yield) as a white solid. ¹H NMR (400 MHz, DMSO-*d*₆) δ 10.36 (s, 1H), 9.84 (s, 1H), 8.10 (d, *J* = 1.4 Hz, 1H), 8.02 (d, *J* = 1.4 Hz, 1H), 7.65 (t, *J* = 2.0 Hz, 1H), 7.51 (dt, *J* = 8.0, 1.3 Hz, 1H), 7.30 (t, *J* = 8.1 Hz, 1H), 7.00–6.85 (m, 1H), 3.01 (s, 3H). ¹³C NMR (75 MHz, DMF-*d*₇) δ 159.2, 141.8, 140.1, 139.7, 131.2, 129.9, 129.8, 115.9, 115.6, 111.8, 109.4, 38.9. LC-MS Purity 95%. LC-MS (ESI+) 377.00.

Synthesis of 4-Bromo-*N*-(3-methanesulfonamidophenyl)-5-methylthiophene-2-carboxamide (9). Following the procedure for **1**, purification by reverse phase column chromatography (5–95% MeCN/H₂O, acidic conditions) afforded 4-bromo-*N*-(3-methanesulfonamidophenyl)-5-methylthiophene-2-carboxamide (**9**, 45.2 mg, 0.116 mmol, 26% yield) as a light yellow solid. ¹H NMR (300 MHz, DMSO-*d*₆) δ 10.27 (s, 1H), 9.81 (s, 1H), 8.03 (s, 1H), 7.65 (t, *J* = 2.1 Hz, 1H), 7.50 (ddd, *J* = 8.2, 2.1, 1.0 Hz, 1H), 7.30 (t, *J* = 8.1 Hz, 1H), 6.94 (ddd, *J* = 8.1, 2.2, 1.0 Hz, 1H), 3.01 (s, 3H), 2.43 (s, 3H). LC-MS Purity 98.4%. LC-MS (ESI+) 389.

Synthesis of *N*-(3-Methanesulfonamidophenyl)-4-phenylthiophene-2-carboxamide (10). **Step 1: Synthesis of Methyl 4-Phenylthiophene-2-carboxylate.** To a mixture of methyl 4-bromothiophene-2-carboxylate (30 g, 135 mmol), phenylboronic acid (32.9 g, 270 mmol, 2 equiv), Pd(dppf)Cl₂ (11.0 g, 13.5 mmol, 0.1 equiv) and K₃PO₄ (85.8 g, 405 mmol, 3 equiv) was added 1,4-dioxane (300 mL) and water (30 mL). The resulting mixture was stirred for 2 h at 80 °C under N₂ atmosphere. The reaction mixture was extracted with EtOAc. The organic extract was concentrated under reduced pressure. The residue was purified by silica gel column chromatography (20% EtOAc/PE) to afford methyl 4-phenylthiophene-2-carboxylate (27.1 g, 124 mmol, 92% yield) as a light yellow solid. ¹H NMR (300 MHz, DMSO-*d*₆) δ 8.19 (d, *J* = 1.7 Hz, 1H), 8.12 (d, *J* = 1.7 Hz, 1H), 7.79–7.72 (m, 2H), 7.43 (dd, *J* = 8.3, 6.6 Hz, 2H), 7.37–7.29 (m, 1H), 3.59 (s, 3H). LC-MS (ESI+) 219.

Step 2: Synthesis of 4-Phenylthiophene-2-carboxylic Acid. To a stirred solution of methyl 4-phenylthiophene-2-carboxylate (26.1 g, 119 mmol) in 260 mL of THF and 260 mL of water was added lithium hydroxide (24.9 g, 595 mmol, 5 equiv). The resulting mixture was stirred overnight at room temperature. The reaction mixture was concentrated, and the pH value of the residual solution was adjusted to 3 with 1 M HCl (aq). Filtration of the precipitated product provided 4-phenylthiophene-2-carboxylic acid (24.4 g, 119 mmol, >99% yield) as a white solid. LC-MS (ESI+) 205.

Step 3: Synthesis of *N*-(3-Methanesulfonamidophenyl)-4-phenylthiophene-2-carboxamide (10). To a stirred solution of *N*-(3-aminophenyl)methanesulfonamide (0.10 g, 0.27 mmol), HATU (0.255 g, 0.670 mmol, 2.5 equiv) and DIPEA (0.2 g, 1.54 mmol, 5.7 equiv) in DMF (5 mL) was added 4-phenylthiophene-2-carboxylic acid (0.109 g, 0.534 mmol, 2 equiv). The mixture was stirred for 12 h

at rt. The mixture was concentrated and purified by reverse phase column chromatography (5–95% MeCN/H₂O, acidic conditions) to afford *N*-(3-methanesulfonamidophenyl)-4-phenylthiophene-2-carboxamide (**10**, 52.1 mg, 0.140 mmol, 52% yield) as an off-white solid. ¹H NMR (400 MHz, DMSO-*d*₆) δ 10.34 (s, 1H), 9.82 (s, 1H), 8.49 (d, *J* = 1.5 Hz, 1H), 8.19 (d, *J* = 1.4 Hz, 1H), 7.79–7.72 (m, 2H), 7.69 (t, *J* = 2.1 Hz, 1H), 7.56–7.44 (m, 3H), 7.40–7.28 (m, 2H), 6.95 (ddd, *J* = 8.0, 2.2, 0.9 Hz, 1H), 3.02 (s, 3H). ¹³C NMR (101 MHz, DMF-*d*₇) δ 162.6, 162.5, 162.3, 162.0, 160.4, 142.7, 141.4, 140.4, 139.7, 135.3, 129.8, 129.3, 127.9, 129.3, 127.86, 127.84, 126.6, 126.3, 115.9, 115.4, 111.8, 38.9. LC-MS Purity 98.4%. HRMS (ESI+) 373.0690.

Synthesis of *N*-(3-Methanesulfonamidophenyl)-4-(pyridin-2-yl)thiophene-2-carboxamide (11). **Step 1: Synthesis of *N*-(3-Methanesulfonamidophenyl)-4-(4,4,5,5-tetramethyl-1,3,2-dioxaborolan-2-yl)thiophene-2-carboxamide.** A solution of 4-bromo-*N*-(3-methanesulfonamidophenyl)thiophene-2-carboxamide (400 mg, 1.07 mmol, 1 equiv), bis(pinacolato)diboron (2.707 g, 10.66 mmol, 10 equiv), Pd(dppf)Cl₂ (77.99 mg, 0.107 mmol, 0.1 equiv) and potassium acetate (313.84 mg, 3.198 mmol, 3 equiv) in 1,4-dioxane (5 mL) was stirred for 2 h at 80 °C under nitrogen atmosphere. The residue was purified by silica gel column chromatography (1:1 PE:EtOAc) to afford *N*-(3-methanesulfonamidophenyl)-4-(4,4,5,5-tetramethyl-1,3,2-dioxaborolan-2-yl)thiophene-2-carboxamide (352 mg, 0.833 mmol, 78% yield) as a yellow oil. LC-MS (ESI+) 423.

Step 2: Synthesis of *N*-(3-Methanesulfonamidophenyl)-4-(pyridin-2-yl)thiophene-2-carboxamide (11). A solution of *N*-(3-methanesulfonamidophenyl)-4-(4,4,5,5-tetramethyl-1,3,2-dioxaborolan-2-yl)thiophene-2-carboxamide (352 mg, 0.833 mmol, 1.5 equiv), 2-bromopyridine (87.79 mg, 0.555 mmol), Pd(dppf)Cl₂ (40.66 mg, 0.056 mmol, 0.1 equiv) and potassium carbonate (230.39 mg, 1.666 mmol, 3 equiv) in 1,4-dioxane (3 mL) and water (1 mL) was stirred for 2 h at 80 °C under nitrogen atmosphere. The residue was purified by reverse phase column chromatography (0–100% MeCN/water) to afford *N*-(3-methanesulfonamidophenyl)-4-(pyridin-2-yl)thiophene-2-carboxamide (**11**, 68.8 mg, 0.184 mmol, 33% yield) as a white solid. ¹H NMR (300 MHz, DMSO-*d*₆) δ 10.48 (s, 1H), 9.81 (s, 1H), 8.75 (d, *J* = 1.4 Hz, 1H), 8.65 (m, *J* = 4.8, 1.4 Hz, 1H), 8.49 (d, *J* = 1.3 Hz, 1H), 7.96–7.88 (m, 2H), 7.73 (t, *J* = 2.0 Hz, 1H), 7.58–7.51 (m, 1H), 7.42–7.28 (m, 2H), 6.95 (m, *J* = 8.1, 2.1, 1.0 Hz, 1H), 3.02 (s, 3H). LC-MS Purity 98.05%. LC-MS (ESI+) 374.1.

Synthesis of *N*-(3-Methanesulfonamidophenyl)-4-(pyridin-3-yl)thiophene-2-carboxamide (12). A solution of 4-bromo-*N*-(3-methanesulfonamidophenyl)thiophene-2-carboxamide (100 mg, 0.266 mmol, 1 equiv), pyridin-3-ylboronic acid (98.27 mg, 0.798 mmol, 3 equiv), Pd(PPh₃)₂Cl₂ (18.70 mg, 0.027 mmol, 0.1 equiv) and Na₂CO₃ (84.73 mg, 0.798 mmol, 3 equiv) in EtOH (3 mL) and water (1 mL) was stirred for 2 h at 80 °C under nitrogen atmosphere. The residue was purified by reverse phase column chromatography (0–100% MeCN/H₂O) to afford *N*-(3-methanesulfonamidophenyl)-4-(pyridin-3-yl)thiophene-2-carboxamide (**12**, 24.4 mg, 0.0653 mmol, 25% yield) as a white solid. ¹H NMR (300 MHz, DMSO-*d*₆) δ 10.35 (s, 1H), 9.83 (s, 1H), 9.01 (m, *J* = 2.4, 0.9 Hz, 1H), 8.65–8.49 (m, 2H), 8.35 (d, *J* = 1.4 Hz, 1H), 8.14 (m, *J* = 8.0, 2.4, 1.6 Hz, 1H), 7.69 (t, *J* = 2.1 Hz, 1H), 7.59–7.48 (m, 2H), 7.33 (t, *J* = 8.1 Hz, 1H), 6.96 (m, *J* = 8.0, 2.1, 1.0 Hz, 1H), 3.02 (s, 3H). LC-MS Purity 99.85%. LC-MS (ESI+) 374.05.

Synthesis of *N*-(3-Methanesulfonamidophenyl)-4-(pyridin-4-yl)thiophene-2-carboxamide (13). Following the procedure for **12**, *N*-(3-methanesulfonamidophenyl)-4-(pyridin-4-yl)thiophene-2-carboxamide (**13**, 23.3 mg, 0.0624 mmol, 23% yield) was obtained as a white solid. ¹H NMR (300 MHz, DMSO-*d*₆) δ 10.40 (s, 1H), 9.83 (s, 1H), 8.75–8.63 (m, 2H), 8.59 (d, *J* = 1.5 Hz, 1H), 8.51 (d, *J* = 1.4 Hz, 1H), 7.80–7.72 (m, 2H), 7.69 (t, *J* = 2.1 Hz, 1H), 7.53 (d, *J* = 8.5 Hz, 1H), 7.33 (t, *J* = 8.1 Hz, 1H), 7.02–6.93 (m, 1H), 3.03 (s, 3H). LC-MS Purity 99.21%. LC-MS (ESI+) 374.1.

Synthesis of *N*-(3-Methanesulfonamidophenyl)-4-(2-methoxyphenyl)thiophene-2-carboxamide (14). A mixture of 4-bromo-*N*-(3-methanesulfonamidophenyl)thiophene-2-carboxamide (100 mg, 0.26 mmol), (2-methoxyphenyl)boronic acid (121 mg, 0.80

mmol, 3 equiv), K_2CO_3 (323 mg, 0.78 mmol, 3 equiv) and $Pd(dppf)Cl_2$ (14 mg, 0.02 mmol, 0.1 equiv) in 4 mL of 1,4-dioxane was stirred for 3 h at 80 °C under a nitrogen atmosphere. It was then quenched with 10 mL of water and extracted with EtOAc (3 × 20 mL), and the combined organic extracts were dried over anhydrous Na_2SO_4 . After filtration, the filtrate was concentrated under reduced pressure. The residue was purified by silica gel column chromatography (50% EtOAc/PE) to afford *N*-(3-methanesulfonamidophenyl)-4-(2-methoxyphenyl)thiophene-2-carboxamide (**14**, 11.3 mg, 0.0281 mmol, 10% yield) as a white solid. 1H NMR (300 MHz, DMSO- d_6) δ 10.30 (s, 1H), 9.79 (s, 1H), 8.40 (d, J = 1.4 Hz, 1H), 8.06 (d, J = 1.3 Hz, 1H), 7.68 (t, J = 2.1 Hz, 1H), 7.62–7.46 (m, 2H), 7.42–7.25 (m, 2H), 7.15 (dd, J = 8.4, 1.1 Hz, 1H), 7.06 (td, J = 7.5, 1.2 Hz, 1H), 6.95 (ddd, J = 8.0, 2.2, 1.0 Hz, 1H), 3.88 (s, 3H), 3.01 (s, 3H). LC-MS Purity 99.2%. LC-MS (ESI+) 403.07.

Synthesis of 4-(2-Fluorophenyl)-N-(3-methanesulfonamidophenyl)thiophene-2-carboxamide (15). Following the procedure for **14**, purification by silica gel column chromatography (0–100% EtOAc/PE) afforded 4-(2-fluorophenyl)-*N*-(3-methanesulfonamidophenyl)thiophene-2-carboxamide (**15**, 49.4 mg, 0.127 mmol, 47% yield) as a white solid. 1H NMR (300 MHz, DMSO- d_6) δ 10.38 (s, 1H), 9.82 (s, 1H), 8.45 (d, J = 1.5 Hz, 1H), 8.15 (t, J = 1.4 Hz, 1H), 7.76 (td, J = 7.7, 1.6 Hz, 1H), 7.69 (t, J = 2.1 Hz, 1H), 7.53 (dt, J = 8.3, 1.4 Hz, 1H), 7.49–7.34 (m, 2H), 7.38–7.30 (m, 1H), 7.31 (d, J = 8.1 Hz, 1H), 7.01–6.92 (m, 1H), 3.02 (s, 3H). LC-MS Purity 99.83%. LC-MS (ESI+) 391.10.

Synthesis of 4-(2,6-Difluorophenyl)-N-(3-methanesulfonamidophenyl)thiophene-2-carboxamide (16). Following the procedure for **14** with 10 mol % XPhosPdG3 as catalyst, purification by silica gel column chromatography (0–100% EtOAc/PE) afforded 4-(2,6-difluorophenyl)-*N*-(3-methanesulfonamidophenyl)thiophene-2-carboxamide (**16**, 69.5 mg, 0.170 mmol, 64% yield) as a white solid. 1H NMR (300 MHz, DMSO- d_6) δ 10.39 (s, 1H), 9.81 (s, 1H), 8.31 (q, J = 1.5 Hz, 1H), 8.12 (q, J = 1.3 Hz, 1H), 7.68 (t, J = 2.0 Hz, 1H), 7.58–7.42 (m, 2H), 7.30 (dt, J = 10.7, 8.2 Hz, 3H), 6.96 (ddd, J = 8.1, 2.2, 1.0 Hz, 1H), 3.02 (s, 3H). LC-MS Purity (99.57%). LC-MS (ESI+) 409.05.

Synthesis of 4-(3-Fluorophenyl)-N-(3-methanesulfonamidophenyl)thiophene-2-carboxamide (17). Following the procedure for **14**, purification by silica gel column chromatography (0–100% EtOAc/PE) afforded 4-(3-fluorophenyl)-*N*-(3-methanesulfonamidophenyl)thiophene-2-carboxamide (**17**, 62.8 mg, 0.161 mmol, 60% yield) as a white solid. 1H NMR (300 MHz, DMSO- d_6) δ 10.32 (s, 1H), 9.83 (s, 1H), 8.52 (d, J = 1.5 Hz, 1H), 8.30 (d, J = 1.4 Hz, 1H), 7.69 (t, J = 2.0 Hz, 1H), 7.66–7.46 (m, 4H), 7.33 (t, J = 8.1 Hz, 1H), 7.26–7.13 (m, 1H), 6.96 (dd, J = 7.7, 2.2 Hz, 1H), 3.03 (s, 3H). LC-MS Purity 99.93%. LC-MS (ESI+) 391.10.

Synthesis of 4-(3-Cyanophenyl)-N-(3-methanesulfonamidophenyl)thiophene-2-carboxamide (18). Following the procedure for **14**, purification by silica gel column chromatography (0–100% EtOAc/PE) afforded 4-(3-cyanophenyl)-*N*-(3-methanesulfonamidophenyl)thiophene-2-carboxamide (**18**, 22.9 mg, 0.0576 mmol, 22% yield) as a white solid. 1H NMR (300 MHz, DMSO- d_6) δ 10.33 (s, 1H), 9.84 (s, 1H), 8.56 (d, J = 1.5 Hz, 1H), 8.39 (d, J = 1.4 Hz, 1H), 8.24 (t, J = 1.7 Hz, 1H), 8.10 (dt, J = 7.9, 1.5 Hz, 1H), 7.83 (dt, J = 7.7, 1.4 Hz, 1H), 7.76–7.65 (m, 2H), 7.52 (ddd, J = 8.2, 2.1, 1.0 Hz, 1H), 7.33 (t, J = 8.1 Hz, 1H), 6.97 (ddd, J = 8.0, 2.2, 1.0 Hz, 1H), 3.03 (s, 3H). LC-MS Purity 99.83%. LC-MS (ESI+) 398.05.

Synthesis of 4-(4-Methylpyridin-3-yl)-N-(3-(methylsulfonamido)phenyl)thiophene-2-carboxamide (19). Following the procedure for **14**, purification by silica gel column chromatography (40% EtOAc/PE) afforded 4-(4-methylpyridin-3-yl)-*N*-(3-(methylsulfonamido)phenyl)thiophene-2-carboxamide (**19**, 24.0 mg, 0.0619 mmol, 21% yield) as an off-white solid. 1H NMR (300 MHz, DMSO- d_6) δ 10.29 (s, 1H), 9.81 (s, 1H), 8.54 (s, 1H), 8.44 (d, J = 5.0 Hz, 1H), 8.23 (d, J = 1.5 Hz, 1H), 8.01 (d, J = 1.4 Hz, 1H), 7.66 (t, J = 2.1 Hz, 1H), 7.50 (dt, J = 8.4, 1.2 Hz, 1H), 7.37 (s, 1H), 7.36–7.25 (m, 1H), 7.02–6.90 (m, 1H), 3.01 (s, 3H), 2.40 (s, 3H). LC-MS Purity 99.3%. LC-MS (ESI+) 388.05.

Synthesis of N-(3-methanesulfonamidophenyl)-4-(5-methoxy-2-methylphenyl)thiophene-2-carboxamide (20). Following the procedure for **14**, purification by reverse phase column chromatography (0–100% MeCN/water, acidic conditions) afforded *N*-(3-methanesulfonamidophenyl)-4-(5-methoxy-2-methylphenyl)thiophene-2-carboxamide (**20**, 22.5 mg, 0.0540 mmol, 27% yield) as a white solid. 1H NMR (300 MHz, DMSO- d_6) δ 10.26 (s, 1H), 9.79 (s, 1H), 8.16 (d, J = 1.4 Hz, 1H), 7.81 (d, J = 1.3 Hz, 1H), 7.67 (t, J = 2.1 Hz, 1H), 7.55–7.46 (m, 1H), 7.31 (t, J = 8.1 Hz, 1H), 7.10 (d, J = 8.2 Hz, 1H), 7.00–6.90 (m, 1H), 6.77 (d, J = 2.6 Hz, 1H), 6.70 (dd, J = 8.2, 2.6 Hz, 1H), 3.81 (s, 3H), 3.01 (s, 3H), 2.24 (s, 3H). LC-MS Purity 99.6%. LC-MS (ESI+) 417.09.

Synthesis of N-(3-Methanesulfonamidophenyl)-5-methyl-4-(pyridin-2-yl)thiophene-2-carboxamide (21). A solution of 4-bromo-*N*-(3-methanesulfonamidophenyl)-5-methylthiophene-2-carboxamide (**9**, 300 mg, 0.770 mmol), 2-(tributylstannyl)pyridine (563 mg, 1.53 mmol, 2 equiv) and $Pd(PPh_3)_4$ (177 mg, 0.154 mmol, 0.2 equiv) in toluene (5 mL) was stirred for 2 h at 120 °C under nitrogen atmosphere. The mixture was concentrated under reduced pressure. Purification of the residue by silica gel column chromatography (0–100% EtOAc/PE) afforded *N*-(3-methanesulfonamidophenyl)-5-methyl-4-(pyridin-2-yl)thiophene-2-carboxamide (**21**, 28.8 mg, 0.0743 mmol, 10% yield) as a yellow solid. 1H NMR (300 MHz, DMSO- d_6) δ 10.31 (s, 1H), 9.79 (s, 1H), 8.69 (ddd, J = 4.8, 1.9, 0.9 Hz, 1H), 8.40 (s, 1H), 7.93 (td, J = 7.7, 1.9 Hz, 1H), 7.75–7.66 (m, 2H), 7.57–7.47 (m, 1H), 7.37 (ddd, J = 7.5, 4.8, 1.1 Hz, 1H), 7.30 (t, J = 8.1 Hz, 1H), 6.93 (ddd, J = 8.0, 2.2, 1.0 Hz, 1H), 3.01 (s, 3H), 2.71 (s, 3H). LC-MS Purity 99.7%. LC-MS (ESI+) 388.10.

Synthesis of N-(3-Methanesulfonamidophenyl)-5-methyl-4-phenylthiophene-2-carboxamide (22). Following the procedure for **14** and starting from bromide **9**, purification by silica gel column chromatography (0–100% EtOAc/PE) afforded *N*-(3-methanesulfonamidophenyl)-5-methyl-4-phenylthiophene-2-carboxamide (**22**, 17.1 mg, 0.0442 mmol, 20% yield). 1H NMR (300 MHz, DMSO- d_6) δ 10.20 (s, 1H), 9.79 (s, 1H), 8.10 (s, 1H), 7.67 (t, J = 2.0 Hz, 1H), 7.54–7.46 (m, 5H), 7.45–7.36 (m, 1H), 7.30 (t, J = 8.1 Hz, 1H), 6.98–6.89 (m, 1H), 3.01 (s, 3H), 2.54 (s, 3H). LC-MS Purity 98.9%. LC-MS (ESI+) 387.05.

Synthesis of N-(3-Bromo-5-methanesulfonamidophenyl)-4-phenylthiophene-2-carboxamide (23). To a mixture of 4-phenylthiophene-2-carboxylic acid (10.1 g, 49.6 mmol, 1.2 equiv) and *N*-(3-amino-5-bromophenyl)methanesulfonamide (11 g, 41.4 mmol) in MeCN (110 mL) was added TCFH (17.3 g, 62.1 mmol, 1.5 equiv) and NMI (10.1 g, 124 mmol, 3 equiv) at rt. The resulting mixture was stirred overnight and then concentrated in vacuo. The residue was purified by reverse phase column chromatography (60% MeCN/0.1% aq formic acid) to afford *N*-(3-bromo-5-methanesulfonamidophenyl)-4-phenylthiophene-2-carboxamide (**23**, 11.1 g, 24.5 mmol, 59% yield) as a light yellow solid. 1H NMR (300 MHz, DMSO- d_6) δ 10.46 (s, 1H), 10.09 (s, 1H), 8.49 (d, J = 1.5 Hz, 1H), 8.23 (d, J = 1.4 Hz, 1H), 7.96–7.60 (m, 4H), 7.57–7.24 (m, 3H), 7.11 (t, J = 1.9 Hz, 1H), 3.08 (s, 3H). ^{13}C NMR (101 MHz, DMF- d_7) δ 160.7, 142.8, 141.7, 141.2, 140.8, 135.2, 129.3, 128.2, 127.9, 127.1, 126.3, 122.3, 118.0, 117.3, 109.7, 39.2. LC-MS Purity 99.0%. HRMS (ESI+) 450.9787.

Synthesis of N-(3-Methanesulfonamido-5-methylphenyl)-4-phenylthiophene-2-carboxamide (24). To a mixture of *N*-(3-amino-5-methylphenyl)-4-phenylthiophene-2-carboxamide (82 mg, 0.265 mmol) and methanesulfonic anhydride (55.3 mg, 0.318 mmol) in MeCN (1 mL) was added TCFH (111 mg, 0.397 mmol) and NMI (65.1 mg, 0.795 mmol). The resulting mixture was stirred at room temperature for 2 h. The reaction mixture was concentrated, and the residue was purified by reverse phase column chromatography (55% MeCN/0.1% aq 0.1% NH_4HCO_3) to afford *N*-(3-methanesulfonamido-5-methylphenyl)-4-phenylthiophene-2-carboxamide (34.0 mg, 0.088 mmol, 33% yield) as a white solid. 1H NMR (300 MHz, DMSO- d_6) δ 10.26 (s, 1H), 9.76 (s, 1H), 8.50 (d, J = 1.5 Hz, 1H), 8.19 (d, J = 1.4 Hz, 1H), 7.80–7.71 (m, 2H), 7.55–7.43 (m, 3H), 7.42–7.30 (m, 2H), 6.79 (d, J = 2.3 Hz, 1H), 3.01 (s, 3H), 2.30 (s, 3H). ^{13}C NMR (76 MHz, DMF- d_7) δ 160.39, 142.72, 141.50, 140.24, 139.60, 139.56, 135.31, 129.32, 127.86, 127.78, 126.61, 126.29,

116.55, 116.12, 109.09, 38.89, 21.25. LC-MS Purity 99.8%. LC-MS (ESI+) 387.15.

Synthesis of *N*-(3-Chloro-5-methanesulfonamidophenyl)-4-(3-methylpyridin-2-yl)thiophene-2-carboxamide (ATX968). Step 1: **Synthesis of Methyl 4-(4,4,5,5-Tetramethyl-1,3,2-dioxaborolan-2-yl)thiophene-2-carboxylate.** A mixture of methyl 4-bromothiophene-2-carboxylate (200 g, 905 mmol), potassium acetate (177.58 g, 1809.4 mmol, 2 equiv), bis(pinacolato)diboron (344.61 g, 1357.0 mmol, 1.5 equiv) and Pd(dppf)Cl₂ (33.10 g, 45.24 mmol, 0.05 equiv) in 1,4-dioxane (2.4 L) was stirred overnight at 80 °C under nitrogen atmosphere. The resulting mixture was concentrated under reduced pressure. The residue was purified by silica gel column chromatography (10:1 PE:EtOAc) to afford methyl 4-(4,4,5,5-tetramethyl-1,3,2-dioxaborolan-2-yl)thiophene-2-carboxylate (210 g, 783 mmol, 87% yield) as a white solid. LC-MS (ESI+) 269.

Step 2: Synthesis of Methyl 4-(3-Methylpyridin-2-yl)thiophene-2-carboxylate. A mixture of methyl 4-(4,4,5,5-tetramethyl-1,3,2-dioxaborolan-2-yl)thiophene-2-carboxylate (210 g, 783 mmol, 1 equiv), 2-bromo-3-methylpyridine (161.68 g, 939.84 mmol, 1.2 equiv), Pd(dppf)Cl₂ (28.65 g, 39.16 mmol, 0.05 equiv) and K₃PO₄ (332.49 g, 1566.4 mmol, 2 equiv) in 1,4-dioxane (2 L) and water (400 mL) was stirred overnight at 80 °C under nitrogen atmosphere. The resulting mixture was diluted with water (2 L) and extracted with EtOAc (3 × 1.5 L) and dried over anhydrous Na₂SO₄. After filtration, the filtrate was concentrated under reduced pressure. The residue was purified by silica gel column chromatography (3:1 PE:EtOAc) to afford methyl 4-(3-methylpyridin-2-yl)thiophene-2-carboxylate (160 g, 686 mmol, 88% yield) as a colorless oil. LC-MS (ESI+) 234.

Step 3: Synthesis of 4-(3-Methylpyridin-2-yl)thiophene-2-carboxylic Acid. A mixture of methyl 4-(3-methylpyridin-2-yl)thiophene-2-carboxylate (160 g, 686 mmol) and LiOH (49.28 g, 2.056 mol, 3 equiv) in EtOH (1 L) and water (250 mL) was stirred for 2 h at room temperature. The mixture was acidified to pH 6 with 2 M HCl (aq). The precipitated solids were collected by filtration and washed with MeCN (2 × 200 mL). This resulted in 4-(3-methylpyridin-2-yl)thiophene-2-carboxylic acid (100 g, 456 mmol, 67% yield) as a white solid. LC-MS (ESI+) 220.

Step 4: Synthesis of *N*-(3-Chloro-5-methanesulfonamidophenyl)-4-(3-methylpyridin-2-yl)thiophene-2-carboxamide (ATX968). A mixture of 4-(3-methylpyridin-2-yl)thiophene-2-carboxylic acid (100 g, 456 mmol), TCFH (383.90 g, 1.3682 mol, 3 equiv) and NMI (187.23 g, 2.2804 mol, 5 equiv) in MeCN (1.5 L) was stirred at 0 °C. *N*-(3-Amino-5-chlorophenyl)methanesulfonamide (100.64 g, 456.08 mmol, 1 equiv) was added to the mixture, which was then stirred overnight at rt. The resulting mixture was diluted with water and extracted with EtOAc (2 × 1.2 L). The combined organic extracts were washed with water (3 × 1 L), dried over anhydrous Na₂SO₄, filtered and concentrated under reduced pressure. The residue was purified by reverse phase column chromatography (10–50% MeCN/H₂O, basic conditions) to afford *N*-(3-chloro-5-methanesulfonamidophenyl)-4-(3-methylpyridin-2-yl)thiophene-2-carboxamide (ATX968, 106.4 g, 252.2 mmol, 55% yield) as an off-white solid. ¹H NMR (400 MHz, Methanol-*d*₄) δ 8.51–8.41 (m, 1H), 8.20 (s, 1H), 8.05–7.94 (m, 1H), 7.83 (d, *J* = 7.8 Hz, 1H), 7.66 (t, *J* = 2.0 Hz, 1H), 7.58 (t, *J* = 2.0 Hz, 1H), 7.37 (m, *J* = 7.8, 4.9 Hz, 1H), 7.03 (t, *J* = 2.0 Hz, 1H), 3.04 (s, 3H), 2.49 (s, 3H). ¹³C NMR (101 MHz, Methanol-*d*₄) δ 161.01, 152.06, 145.63, 140.75, 140.39, 140.17, 139.92, 139.28, 134.66, 132.29, 131.38, 129.98, 123.01, 115.82, 114.85, 109.72, 38.19, 18.87. HPLC Purity 98.39%. HRMS (ESI+) 422.0419.

Synthesis of *N*-(3-Bromo-5-methanesulfonamidophenyl)-4-(pyridin-2-yl)thiophene-2-carboxamide (25). Following the procedure for ATX968, purification by silica gel column chromatography (10% MeOH/DCM) followed by triturated with 300 mL of 30% MeOH/DCM afforded *N*-(3-bromo-5-methanesulfonamidophenyl)-4-(pyridin-2-yl)thiophene-2-carboxamide (25, 54.8 g, 121 mmol, 19% yield) as a white solid. ¹H NMR (300 MHz, DMSO-*d*₆) δ 10.61 (s, 1H), 10.08 (s, 1H), 8.75 (d, *J* = 1.4 Hz, 1H), 8.65 (m, *J* = 4.8, 1.4 Hz, 1H), 8.52 (d, *J* = 1.3 Hz, 1H), 7.92 (m, *J* = 2.9, 1.4 Hz, 2H), 7.84 (t, *J* = 1.8 Hz, 1H), 7.75 (t, *J* = 1.9 Hz, 1H), 7.36 (td, *J* = 5.3, 3.1 Hz, 1H), 7.10 (t, *J* = 1.8 Hz, 1H), 3.08 (s, 3H). ¹³C NMR (101 MHz, DMSO-

*d*₆) δ 160.26, 152.40, 149.55, 142.81, 141.36, 140.73, 140.43, 137.04, 129.21, 128.03, 122.42, 121.89, 119.97, 117.62, 116.92, 109.40, 40.27. HPLC Purity 97.85%. LC-MS (ESI+) 452.00.

Synthesis of *N*-(3-Chloro-5-methanesulfonamidophenyl)-4-(pyridin-2-yl)thiophene-2-carboxamide (26). Step 1: **Synthesis of Methyl 4-(4,4,5,5-Tetramethyl-1,3,2-dioxaborolan-2-yl)thiophene-2-carboxylate.** Following the procedure for ATX968 Step 1, purification by reverse phase column chromatography (5–95% MeCN/H₂O, acidic conditions) afforded methyl 4-(4,4,5,5-tetramethyl-1,3,2-dioxaborolan-2-yl)thiophene-2-carboxylate (310 mg, 1.15 mmol, 95% yield) as a yellow solid. LC-MS (ESI+) 269.

Step 2: Synthesis of Methyl 4-(pyridin-2-yl)thiophene-2-carboxylate. To a stirred solution of methyl 4-(4,4,5,5-tetramethyl-1,3,2-dioxaborolan-2-yl)thiophene-2-carboxylate (310 mg, 1.15 mmol), 2-bromopyridine (363 mg, 2.30 mmol), Pd(PPh₃)Cl₂ (117 mg, 0.115 mmol) and Na₂CO₃ (3650 mg, 3.45 mmol) in EtOH (10.00 mL) was added H₂O (3.00 mL). The mixture was stirred for 12 h at 80 °C. The mixture was concentrated and purified by reverse phase column chromatography (5–95% MeCN/H₂O, acidic conditions) to afford methyl 4-(pyridin-2-yl)thiophene-2-carboxylate (240 mg, 1.09 mmol, 95% yield) as a white solid. LC-MS (ESI+) 220.

Step 3: Synthesis of 4-(Pyridin-2-yl)thiophene-2-carboxylic Acid. To a stirred solution of methyl 4-(pyridin-2-yl)thiophene-2-carboxylate (240 mg, 1.09 mmol) and LiOH (10 mg, 2.5 mmol) in MeOH (10.00 mL) was added H₂O (10.00 mL) dropwise. Then the mixture was stirred for 2 h at rt. The mixture was acidified to pH 5 with citric acid. The precipitated solids were collected by filtration and washed with water. The resulting solid was dried under vacuum to afford 4-(pyridin-2-yl)thiophene-2-carboxylic acid (190 mg, 0.926 mmol, 85% yield) as a yellow solid. LC-MS (ESI+) 206.

Step 4: Synthesis of *N*-(3-Chloro-5-nitrophenyl)-4-(pyridin-2-yl)thiophene-2-carboxamide. To a stirred solution of 4-(pyridin-2-yl)thiophene-2-carboxylic acid (90 mg, 0.438 mmol), TCFH (184.6 mg, 0.657 mmol) and NMI (108 mg, 1.314 mmol) in MeCN (5.00 mL) was added 3-chloro-5-nitroaniline (75.5 mg, 0.438 mmol). The mixture was stirred for 4 h at rt. The mixture was concentrated and purified by reverse phase column chromatography (5–95% MeCN/H₂O, acidic conditions) to afford *N*-(3-chloro-5-nitrophenyl)-4-(pyridin-2-yl)thiophene-2-carboxamide (157 mg, 0.436 mmol, 99% yield) as a yellow solid. LC-MS (ESI+) 360.

Step 5: Synthesis of *N*-(3-Amino-5-chlorophenyl)-4-(pyridin-2-yl)thiophene-2-carboxamide. To a solution of *N*-(3-chloro-5-nitrophenyl)-4-(pyridin-2-yl)thiophene-2-carboxamide (150 mg, 0.416 mmol) in MeOH and water (10 mL) was added Fe (116 mg, 2.08 mmol) and NH₄Cl (222.5 mg, 4.16 mmol). The resulting mixture was stirred for 2 h at 80 °C under N₂ atmosphere. The mixture was filtered. The filtrate was concentrated and purified by silica gel column chromatography (0–100% EtOAc/PE) to afford *N*-(3-amino-5-chlorophenyl)-4-(pyridin-2-yl)thiophene-2-carboxamide (120 mg, 0.364 mmol, 87% yield) as a yellow solid. LC-MS (ESI+) 329.

Step 6: Synthesis of *N*-(3-Chloro-5-methanesulfonamidophenyl)-4-(pyridin-2-yl)thiophene-2-carboxamide (26). To a stirred solution of *N*-(3-amino-5-chlorophenyl)-4-(pyridin-2-yl)thiophene-2-carboxamide (60 mg, 0.181 mmol) in pyridine (5 mL) was added methanesulfonyl chloride (24.8 mg, 0.217 mmol, 1.2 equiv) dropwise at 0 °C. The mixture was stirred for 12 h at room temperature, concentrated and purified by silica gel column chromatography (0–100% EtOAc/PE) to afford *N*-(3-chloro-5-methanesulfonamidophenyl)-4-(pyridin-2-yl)thiophene-2-carboxamide (26, 26.8 mg, 0.0657 mmol, 36% yield) as a white solid. ¹H NMR (400 MHz, DMSO-*d*₆) δ 10.61 (s, 1H), 10.14 (s, 1H), 8.75 (d, *J* = 1.3 Hz, 1H), 8.64 (dt, *J* = 4.8, 1.5 Hz, 1H), 8.51 (d, *J* = 1.3 Hz, 1H), 7.96–7.86 (m, 2H), 7.72–7.66 (m, 2H), 7.36 (ddd, *J* = 6.2, 4.8, 2.5 Hz, 1H), 6.97 (t, *J* = 2.0 Hz, 1H), 3.18 (q, *J* = 7.3 Hz, 2H), 1.22 (t, *J* = 7.3 Hz, 3H). ¹³C NMR (76 MHz, DMF-*d*₇) δ 160.70, 152.82, 149.98, 143.23, 141.66, 141.07, 140.86, 137.47, 134.30, 129.67, 128.45, 122.85, 120.39, 115.04, 114.35, 109.29, 39.22. LC-MS Purity 98.4%. LC-MS (ESI+) 408.05.

Synthesis of *N*-(3-Chloro-5-methanesulfonamidophenyl)-4-(2,6-difluorophenyl)thiophene-2-carboxamide (27). Step 1: **Synthesis of *N*-(3-Amino-5-chlorophenyl)-4-bromothiophene-2-carboxamide.**

Following the procedure for **26** Step 1, purification by silica gel column chromatography (0–100% EtOAc/PE) afforded 4-bromo-*N*-(3-chloro-5-nitrophenyl)thiophene-2-carboxamide (3.2 g, 8.8 mmol, 95% yield) as a yellow solid. LC-MS (ESI+) 361.

Step 2: Synthesis of *N*-(3-Amino-5-chlorophenyl)-4-bromothiophene-2-carboxamide. Following the procedure for **26** Step 2, silica gel column chromatography (0–100% EtOAc/PE) afforded *N*-(3-amino-5-chlorophenyl)-4-bromothiophene-2-carboxamide (2.93 g, 8.8 mmol, 95% yield) as a yellow solid. LC-MS (ESI) [M + H]⁺: 331.

Step 3: Synthesis of 4-Bromo-*N*-(3-chloro-5-methanesulfonamidophenyl)thiophene-2-carboxamide. Following the procedure for **26** Step 3, purification by silica gel column chromatography (0–100% EtOAc/PE) afforded 4-bromo-*N*-(3-chloro-5-methanesulfonamidophenyl)thiophene-2-carboxamide (800 mg, 1.95 mmol, 95% yield) as a yellow solid. LC-MS (ESI+) 409.

Step 4: Synthesis of *N*-(3-Chloro-5-methanesulfonamidophenyl)-4-(2,6-difluorophenyl)thiophene-2-carboxamide (27**).** A mixture of 4-bromo-*N*-(3-chloro-5-methanesulfonamidophenyl)thiophene-2-carboxamide (100 mg, 0.244 mmol), 2-(2,6-difluorophenyl)-4,4,5,5-tetramethyl-1,3,2-dioxaborolane (117 mg, 0.488 mmol), XPhosPdG3 (21 mg, 0.0244 mmol) and K₃PO₄ (155 mg, 0.732 mmol) in 1,4-dioxane (5.00 mL) was stirred for 8 h at 80 °C. The mixture was concentrated and purified by reverse phase column chromatography (5–95% MeCN/H₂O, acidic conditions) to afford *N*-(3-chloro-5-methanesulfonamidophenyl)-4-(2,6-difluorophenyl)thiophene-2-carboxamide (31.3 mg, 0.0706 mmol, 29% yield) as an off-white solid. ¹H NMR (300 MHz, DMSO-*d*₆) δ 10.52 (s, 1H), 10.10 (s, 1H), 8.31 (s, 1H), 8.15 (s, 1H), 7.66 (d, *J* = 13.3 Hz, 2H), 7.50 (q, *J* = 7.4 Hz, 1H), 7.28 (t, *J* = 8.2 Hz, 2H), 6.98 (s, 1H), 3.08 (s, 3H). LC-MS Purity 98.2%. LC-MS (ESI+) 443.05.

Synthesis of *N*-(3-Chloro-5-methanesulfonamidophenyl)-4-(2-methoxyphenyl)thiophene-2-carboxamide (28**).** A mixture of 4-bromo-*N*-(3-chloro-5-methanesulfonamidophenyl)thiophene-2-carboxamide (100 mg, 0.244 mmol), (2-methoxyphenyl)boronic acid (74.1 mg, 0.488 mmol), Pd(dppf)Cl₂ (20 mg, 0.0244 mmol) and K₂CO₃ (101 mg, 0.732 mmol) in 1,4-dioxane (5.00 mL) was stirred for 3 h at 80 °C. The mixture was concentrated and purified by reverse phase column chromatography (5–95% MeCN/H₂O, acidic conditions) to afford *N*-(3-chloro-5-methanesulfonamidophenyl)-4-(2-methoxyphenyl)thiophene-2-carboxamide (45.8 mg, 0.105 mmol, 43% yield) as a gray solid. ¹H NMR (400 MHz, DMSO-*d*₆) δ 10.45 (s, 1H), 10.08 (s, 1H), 8.41 (d, *J* = 1.4 Hz, 1H), 8.09 (d, *J* = 1.3 Hz, 1H), 7.66 (dt, *J* = 15.8, 1.9 Hz, 2H), 7.57 (dd, *J* = 7.5, 1.7 Hz, 1H), 7.36 (t, *J* = 8.1 Hz, 1H), 7.15 (d, *J* = 8.2 Hz, 1H), 7.06 (t, *J* = 7.4 Hz, 1H), 6.97 (t, *J* = 1.9 Hz, 1H), 3.87 (s, 3H), 3.07 (s, 3H). LC-MS Purity 99.0%. LC-MS (ESI+) 437.10.

Synthesis of *N*-(3-Chloro-5-methanesulfonamidophenyl)-5-methyl-4-(pyridin-2-yl)thiophene-2-carboxamide (29**).** Following the procedure for **ATX968**, purification by reverse phase column chromatography (5–95% MeCN/H₂O, acidic conditions) provided *N*-(3-chloro-5-methanesulfonamidophenyl)-5-methyl-4-(pyridin-2-yl)thiophene-2-carboxamide (29.2 mg, 0.0692 mmol, 19% yield) as a white solid. ¹H NMR (400 MHz, DMSO-*d*₆) δ 10.45 (s, 1H), 10.09 (s, 1H), 8.69 (s, 1H), 8.40 (s, 1H), 7.93 (s, 1H), 7.69 (d, *J* = 9.9 Hz, 2H), 7.64 (s, 1H), 7.37 (s, 1H), 6.95 (s, 1H), 3.07 (s, 3H), 2.71 (s, 3H). ¹³C NMR (75 MHz, DMF-*d*₇) δ 160.58, 154.24, 149.79, 144.55, 141.75, 141.03, 138.44, 137.18, 135.42, 134.30, 131.17, 122.59, 122.24, 114.95, 114.23, 109.18, 39.22, 15.32. LC-MS Purity 98.8%. LC-MS (ESI+) 422.10.

Synthesis of *N*-(3-Chloro-5-methanesulfonamidophenyl)-5-methyl-4-[5-(trifluoromethyl)pyridin-2-yl]thiophene-2-carboxamide (30**).** Following the procedure for **ATX968**, purification by reverse phase column chromatography (5–95% MeCN/H₂O, acidic conditions) afforded *N*-(3-chloro-5-methanesulfonamidophenyl)-5-methyl-4-[5-(trifluoromethyl)pyridin-2-yl]thiophene-2-carboxamide (**30**, 110.3 mg, 0.225 mmol, 33% yield) as a white solid. ¹H NMR (300 MHz, DMSO-*d*₆) δ 10.51 (s, 1H), 10.09 (s, 1H), 9.07 (s, 1H), 8.48 (s, 1H), 8.40–8.33 (m, 1H), 7.93 (d, *J* = 8.4 Hz, 1H), 7.68 (d, *J* = 1.9 Hz, 1H), 7.64 (s, 1H), 6.96 (t, *J* = 2.0 Hz, 1H), 3.08 (s, 3H), 2.77 (s, 3H). LC-MS Purity 99.9%. LC-MS (ESI+) 489.90.

Synthesis of *N*-(3-Chloro-5-methanesulfonamidophenyl)-4-(5-ethoxyppyridin-2-yl)-5-methylthiophene-2-carboxamide (31**).** Following the procedure for **ATX968**, purification by reverse phase column chromatography (5–95% MeCN/H₂O, acidic conditions) afforded *N*-(3-chloro-5-methanesulfonamidophenyl)-4-(5-ethoxyppyridin-2-yl)-5-methylthiophene-2-carboxamide (**31**, 69.4 mg, 0.149 mmol, 44% yield) as a white solid. ¹H NMR (400 MHz, DMSO-*d*₆) δ 10.42 (s, 2H), 8.40–8.32 (m, 2H), 7.74–7.55 (m, 3H), 7.50 (dd, *J* = 8.7, 3.0 Hz, 1H), 6.94 (t, *J* = 2.0 Hz, 1H), 4.16 (q, *J* = 6.9 Hz, 2H), 3.06 (s, 3H), 2.67 (s, 3H), 1.38 (t, *J* = 6.9 Hz, 3H). LC-MS Purity 99.4%. LC-MS (ESI+) 465.95.

Synthesis of *N*-(3-Chloro-5-(ethylsulfonamido)phenyl)-4-(pyridin-2-yl)thiophene-2-carboxamide (32**).** To a stirred solution of *N*-(3-amino-5-chlorophenyl)-4-(pyridin-2-yl)thiophene-2-carboxamide (60 mg, 0.181 mmol) in pyridine (5.00 mL) was added ethanesulfonyl chloride (46.5 mg, 0.362 mmol) dropwise at 0 °C. Then the mixture was stirred for 12 h at rt. The mixture was concentrated and purified by silica gel column chromatography (0–100% EtOAc/PE) to afford *N*-(3-chloro-5-ethanesulfonamidophenyl)-4-(pyridin-2-yl)thiophene-2-carboxamide (28.9 mg, 0.0685 mmol, 38% yield) as a white solid. ¹H NMR (300 MHz, DMSO-*d*₆) δ 10.61 (s, 1H), 10.14 (s, 1H), 8.75 (d, *J* = 1.4 Hz, 1H), 8.65 (dt, *J* = 4.8, 1.4 Hz, 1H), 8.52 (d, *J* = 1.3 Hz, 1H), 7.97–7.85 (m, 2H), 7.69 (d, *J* = 2.0 Hz, 2H), 7.36 (td, *J* = 5.3, 2.9 Hz, 1H), 6.97 (t, *J* = 1.9 Hz, 1H), 3.18 (dd, *J* = 8.1, 6.6 Hz, 2H), 1.23 (t, *J* = 7.3 Hz, 3H). LC-MS Purity 98.7%. LC-MS (ESI+) 422.15.

Protein Purification. DHX9 constructs (human and cat) used for biochemical and SPR assays and for X-ray crystallography were expressed and purified as previously described.^{12,13}

ATPase Assay. The DHX9 ATPase assay was performed as previously reported,¹² with the exception that reactions were performed in the presence of compounds and allowed to proceed for 60 min prior to being stopped by the addition of ADP-Glo reagent. Briefly, hDHX9 (final concentration (fc) = 0.625 nM) was preincubated with compounds (fc = 28–86 μM, due to variable compound stock concentration for single point experiments; fc = 100 or 10 μM top concentration; 12-point, 3-fold serial dilution for concentration response) for 15 min. Reactions were initiated by adding double-stranded RNA substrate (fc = 15 nM) and ultrapure ATP (fc = 5 μM) substrates and incubated for 60 min. They were stopped by the addition of ADP-Glo reagent and then treated with Kinase Detection Reagent for 45 min. The plates were centrifuged at 800 rpm for 15 s and read on an Envision (PerkinElmer) plate-based reader for total luminescence signal. To identify false positives due to interference with ADP-Glo kit reagents, the ATPase assay was performed in the presence of compounds using a mixture of ATP and ADP (ATP fc = 1 and ADP fc = 4 μM as low control) or ATP (fc = 5 μM as high control) and absence of hDHX9 and RNA substrate. A counter-screen to identify nonspecific aggregators causing inhibition due to compound aggregation was performed in the same ATPase assay with modified assay buffer containing 10× higher Tween 20 concentration (fc = 0.1%). Similarly, a counter-screen to identify compound leading to enzyme aggregation was run the presence of 10× higher concentrations of hDHX9 (fc = 6.25 nM). Each assay was allowed to incubate with compounds for 60 min prior to ADP-Glo and Kinase detection reagent addition as described in the primary assay.

Unwinding Assay. The DHX9 unwinding assay was run as described in with the addition of compounds.¹² For compound screening, DHX9 (fc = 2.5 nM) were added into assay ready plates containing compounds (fc = 100 or 10 μM top concentration; 12-point, 3-fold serial dilution for concentration response) using a Multidrop Combi (Thermo Fisher Scientific) and preincubated for 15 min. Reactions were started by adding ultrapure ATP (fc = 5 μM) and split-beacon oligonucleotide substrate (fc = 12.5 nM). The reaction was read kinetically at 60 s intervals for 30 min on an Envision (PerkinElmer, Waltham, MA) monitoring Cy5 fluorescence signal at a wavelength of 660 nm. Slopes were calculated using the initial velocity phase of the reaction.

circBRIP1 Assay. The circBRIP1 assay was performed as previously described.⁴

LS411N and H747 Proliferation Assays. The antiproliferation assays were performed as previously described.⁴

SPR Assay. The SPR assay was performed as previously described.¹²

Thermal Shift Assay. Samples for melting temperature (T_m) analysis were prepared in 25 mM Hepes pH 7.5, 20 mM KCl, and 1% DMSO. 2 μ M (fc) Human DHX9 (aa 150-1150-FLAG) was mixed with 2.5 μ M (fc) dsRNA substrate from the ATPase assay prior to compound or DMSO (control) addition. Compound 10, 23, or 24 was added to the DHX9-RNA complex at a fc of 1.56, 6.25, 25, and 100 μ M (all samples with matching % DMSO). The thermal shift assay was performed using the Prometheus Panta (Nanotemper) instrument and standard capillaries. The temperature ramp was set to +1 °C/min, from 25 to 95 °C. The ratio of native tryptophan fluorescence at 350 vs 330 nm was used to track unfolding of the DHX9-RNA complex in the presence or absence of compound. The instrument specific analysis software was used to calculate the first derivative of the fluorescent ratio curve (350/330 nm) and a two-state fit of the fluorescent ratio data yielded the T_m . Reported values are from two independent experiments, and each experiment included two technical replicates (capillaries) for each sample.

Crystallization and Structure Determination. Crystals of cat or human DHX9 bound to ADP and compound were obtained by cocrystallization or by soaking of ADP-bound DHX9 crystals with inhibitor, as indicated in Table S6. Samples were prepared in crystallization buffer (25 mM HEPES, 300 mM NaCl, 2 mM TCEP, pH 7.5, 5 mM ADP, 50 mM MgCl₂), with 1 mM inhibitor compound added for cocrystallization experiments. Crystallization drops were generated using the hanging drop vapor diffusion method at 18 °C in the conditions indicated in Table S6, with streak-seeding using crystals generated from ADP-bound DHX9 crystals. To obtain crystals of feline DHX9 bound to ADP and 23, feline DHX9-ADP crystals were soaked with 1 mM 23 for 24 h at 18 °C. Crystals were passed through cryosolution (Table S6) prior to freezing by immersion in liquid nitrogen. Data collection and processing statistics, including data reduction and scaling software used for each structure, are detailed in Table S7. All structures were solved by molecular replacement in Phaser using the crystal structures of ADP-bound cat or human DHX9 (PDB ID codes 8SZQ and 8SZP) and visual inspection of the electron density maps.³⁹ Small molecule coordinate and restraint dictionary files were generated using CORINA Classic (Molecular Networks GmbH) and ligand fitting was performed manually in Coot.⁴⁰ Structure refinement was completed via iterative cycles of refinement and model building using REFMAC5 and Coot, respectively.^{40,41} Validation of the refined structures was performed at the Protein Data Bank validation server (validate.wwpdb.org). Structure determination and refinement statistics are shown in Table S8. The structures have been deposited in the Protein Data Bank (PDB ID codes to be added after publication).

Solubility in FaSSIF Buffer. A buffer was prepared by dissolving NaOH (1.392 g), maleic acid (2.220 g) and NaCl (4.010 g) into approximately 900 mL ultrapure water. The pH was adjusted to 6.5 with 1 M NaOH (aq), then the solution was diluted to 1000 mL with ultrapure water at room temperature. To 500 mL of this buffer was added 1.790 g FaSSIF-V2 powder, and the mixture was stirred until the powder completely dissolved. The resulting solution was then diluted to 1000 mL with buffer. 10 μ L of test sample in 30 mM stock solution in DMSO was added in 990 μ L of FaSSIF buffer in 96-well plate and shaken (Thermomixed Comfort plate shaker, 1100 rpm) at rt for 2 h. After 2 h of incubation, stir sticks were removed magnetically and the samples were filtered using a vacuum manifold. The filtered samples were diluted with MeOH to achieve appropriate concentrations for analysis. Meanwhile, standards for analysis were prepared from 300 μ M DMSO stocks by diluting to 0.3 μ M with MeOH. Soluble test compound was determined by LC-MS/MS.

Mouse Pharmacokinetics. All the procedures related to animal handling, care, and the treatment in this study were performed according to guidelines approved by the Institutional Animal Care

and Use Committee (IACUC) of Pharmaron following the guidance of the Association for Assessment and Accreditation of Laboratory Animal Care (AAALAC) with Animal Utilization Protocol numbers PK-M-07182021 and PK-M-07182024. Pharmaron abided by relevant laws and regulations and globally recognized standards for animal welfare and ethics, including the Regulations on the Administration of Laboratory Animals, and the Laboratory Animal-Requirements of Environment and Housing Facilities, the Animals (Scientific Procedures) Act of 1986 of the UK (amended 2021), and the Animal Welfare Act of the US. In addition, all portions of this study were performed at Pharmaron and adhered to the study protocol approved by the sponsor and applicable standard operating procedures. The pharmacokinetics of test articles were evaluated in either male CD1 or female Balb/C nude mice ($N = 3$ for each experimental arm) following a single iv administration at 3 mg/kg or a single po administration at 10, 100, or 300 mg/kg. All animals were food-fasted overnight prior to dosing and fed 4 h post dose, with free access to water. For all iv administration, the vehicle used was 5% DMSO, 10% Solutol HS-15 and 85% saline. For po administration at 10 mg/kg, the vehicle was 20% Solutol HS-15 in aqueous 0.5% methylcellulose. For po administration at 100 or 300 mg/kg, the vehicle used 20% Solutol HS-15, 50% aq methylcellulose (1%) with 100 mg/mL PVP VA65 and 30% water. Serial blood samples were collected at 0.083, 0.25, 0.5, 1, 2, 4, 6, 8, 12, and 24 h post dose for iv administration, and 0.25, 0.5, 1, 2, 4, 6, 8, 12, and 24 h post dose for po administration. All samples were analyzed by LC-MS/MS after protein precipitation. Individual test article plasma concentrations were used to calculate the pharmacokinetic parameters by employing a noncompartmental analysis (Phoenix WinNonlin). The linear trapezoidal algorithm was used for AUC calculation and the last 3 (nonzero) data points that appeared to be on the terminal phase of the concentration–time curve were used for the calculation of elimination half-life and related data were reported if R-squared was ≥ 0.9 (when rounded) and when the extrapolated area under the curve from the last time point to infinity represented $<30\%$ of the AUC_{inf} . Mean pharmacokinetic parameters were calculated from individual animals and were rounded to a maximum of three significant figures for presentation in the tables.

■ ASSOCIATED CONTENT

Supporting Information

The Supporting Information is available free of charge at <https://pubs.acs.org/doi/10.1021/acs.jmedchem.5c00252>.

Molecular formula strings and including some data (CSV)

Counter assay for hit validation of compound 1; compound 1 biochemical MOI studies; SPR traces of compound 1 and ATX968; superimposed structures of compound 1 bound to human and feline DHX9; thermal shift plots for compounds 10, 23, and 24; concentration–response plots for ATPase and unwinding assays of ATX968; ADME properties of compounds 1, 23, and ATX968; modification of amide/sulfonamide moieties of compound 1; compounds targeting covalent bond to Cys490; tabulated data from thermal shift assay for compounds 10, 23, and 24; mouse PK parameters for dose-escalation studies of ATX968; crystallization conditions; X-ray crystallography data collection and processing statistics; X-ray crystallography structure determination and refinement statistics; synthesis of acid precursor to compound 5; analytical data for compounds 1–32 and ATX968; and synthesis and analytical data for supplemental compounds (PDF)

Accession Codes

Atomic coordinates for the X-ray crystal structures of compounds 1 (PDB 9MFP), 10 (PDB 9MFQ), 23 (PDB

9MFR) and ATX968 (PDB 9MFS) bound to feline DHX9-ADP and compounds 1 (PDB 9MFO) and ATX968 (PDB 9MFT) bound to human DHX9-ADP are available from the RCSB Protein Data Bank (www.rcsb.org). Authors will release the atomic coordinates upon article publication.

AUTHOR INFORMATION

Corresponding Author

Brian A. Sparling – *Accent Therapeutics, Inc., Lexington, Massachusetts 02421, United States*; orcid.org/0000-0001-5184-0956; Email: bsparling@accenttx.com

Authors

Matthew H. Daniels – *Accent Therapeutics, Inc., Lexington, Massachusetts 02421, United States*; Present Address: Psivant Therapeutics, Boston, Massachusetts 02210, United States; orcid.org/0000-0002-2492-9653

Jennifer Castro – *Accent Therapeutics, Inc., Lexington, Massachusetts 02421, United States*

Young-Tae Lee – *Accent Therapeutics, Inc., Lexington, Massachusetts 02421, United States*; orcid.org/0000-0002-3522-9361

Deepali Gotur – *Accent Therapeutics, Inc., Lexington, Massachusetts 02421, United States*

Kevin E. Knockenhauer – *Accent Therapeutics, Inc., Lexington, Massachusetts 02421, United States*

Simina Grigoriu – *Accent Therapeutics, Inc., Lexington, Massachusetts 02421, United States*; orcid.org/0000-0002-5525-7300

Gordon J. Lockbaum – *Accent Therapeutics, Inc., Lexington, Massachusetts 02421, United States*; Present Address: Recludix Pharma, San Diego, California 92121, United States.; orcid.org/0000-0003-2720-6984

Jae Eun Cheong – *Accent Therapeutics, Inc., Lexington, Massachusetts 02421, United States*; Present Address: Monte Rosa Therapeutics, Boston, Massachusetts 02118, United States.

Chuang Lu – *Accent Therapeutics, Inc., Lexington, Massachusetts 02421, United States*; Present Address: BridgeBio, Palo Alto, California 94304, United States.

David Brennan – *Accent Therapeutics, Inc., Lexington, Massachusetts 02421, United States*

Shane M. Buker – *Accent Therapeutics, Inc., Lexington, Massachusetts 02421, United States*; Present Address: Rgenta Therapeutics, Woburn, Massachusetts 01801, United States.

Julie Liu – *Accent Therapeutics, Inc., Lexington, Massachusetts 02421, United States*

Shihua Yao – *Accent Therapeutics, Inc., Lexington, Massachusetts 02421, United States*

E. Allen Sickmier – *Accent Therapeutics, Inc., Lexington, Massachusetts 02421, United States*; Present Address: Recludix Pharma, San Diego, California 92121, United States.

Scott Ribich – *Accent Therapeutics, Inc., Lexington, Massachusetts 02421, United States*; Present Address: Blueprint Medicines, Cambridge, Massachusetts 02139, United States.

Steve J. Blakemore – *Accent Therapeutics, Inc., Lexington, Massachusetts 02421, United States*; Present Address: Bicycle Therapeutics, Cambridge, Massachusetts 02140, United States.

Serena J. Silver – *Accent Therapeutics, Inc., Lexington, Massachusetts 02421, United States*; orcid.org/0000-0001-8090-2941

P. Ann Boriack-Sjodin – *Accent Therapeutics, Inc., Lexington, Massachusetts 02421, United States*; Present Address: Takeda Pharmaceuticals America, Cambridge, Massachusetts 02139, United States.

Kenneth W. Duncan – *Accent Therapeutics, Inc., Lexington, Massachusetts 02421, United States*; orcid.org/0000-0002-3047-7825

Robert A. Copeland – *Accent Therapeutics, Inc., Lexington, Massachusetts 02421, United States*; Present Address: Atlas Venture, Cambridge, Massachusetts 02139, United States.; orcid.org/0000-0002-1897-6533

Complete contact information is available at: <https://pubs.acs.org/10.1021/acs.jmedchem.5c00252>

Notes

The authors declare the following competing financial interest(s): All authors are or were employees of Accent Therapeutics while work was completed and may hold company stocks or stock options with Accent Therapeutics.

ACKNOWLEDGMENTS

The authors thank Pharmaron for synthetic chemistry and support for biochemical assays, cellular assays, in vitro ADME and in vivo studies; SYNthesis (now a part of Viva Biotech) for synthetic chemistry; Charles River Laboratories for SPR support; Viva Biotech for protein preparation and structural biology support; James Mills, Gavin Whitlock, and Karl Gibson from Sandexis Medicinal Chemistry and Andrew Tasker for their insights; Gina Prophete for compound management; and Hyelee Lee for critically reviewing this manuscript.

ABBREVIATIONS

γ H2AX, serine 139 phosphorylated H2A histone family member X; A \rightarrow B, apical to basolateral; AUC_{0–24h}, area under the time concentration curve from time 0 to 24 h post last dose; AUC_{0–24h,u}, unbound area under the time concentration curve from time 0 to 24 h post last dose; circBRIP1, circular BRCA1-interacting protein 1; circRNA, circular RNA; C_{max}, maximum concentration; C_{max,u}, unbound maximum concentration; C_{min}, minimum concentration; CRC, colorectal cancer; DHX9, DEXH-box helicase 9; DIPEA, *N,N*-diisopropylethylamine; dMMR, deficient mismatch repair; dppf, 1,1'-bis(diphenylphosphino)ferrocene; dsRNA, double-stranded RNA; EC₉₀, 90% of maximal effective concentration; EtOAc, ethyl acetate; EtOH, ethanol; FaSSIF, fasted state simulated intestinal fluid; fc, final concentration; GTP γ S, guanosine 5'-O-[gamma-thio]triphosphate; HATU, 1-[bis(dimethylamino)methylene]-1*H*-1,2,3-triazolo[4,5-*b*]pyridinium 3-oxide hexafluorophosphate; K_D, binding constant; k_D, dissociation rate; MeCN, acetonitrile; MeOH, methanol; MOI, mechanism of inhibition; MSI-H, microsatellite instability high; MSS, microsatellite stable; NMI, 1-methylimidazole; PE, petroleum ether; pin, pinacolato; Pd-PEPPSI-iHept-Cl, 3-chloropyridine 4,5-dichloro-1,3-bis[2,6-di(heptan-4-yl)phenyl]-2*H*-imidazol-2-ide dichloropalladium; pMMR, proficient mismatch repair; RPA32, replication protein A 32 kDa subunit; SCLC, small-cell lung cancer; SD., standard deviation; sol., solubility; SPR, surface plasmon resonance; ssRNA, single-stranded RNA; TCFH, *N,N,N',N'*-tetramethyl-

chloroformamidinium hexafluorophosphate; VDW, van der Waals; XPhosPdG3, (2-dicyclohexylphosphino-2',4',6'-triisopropyl-1,1'-biphenyl)[2-(2'-amino-1,1'-biphenyl)]palladium-(II) methanesulfonate

REFERENCES

- (1) Gulliver, C.; Hoffmann, R.; Baillie, G. S. The Enigmatic Helicase DHX9 and Its Association With the Hallmarks of Cancer. *Future Sci. OA* **2021**, *7* (2), FSO650.
- (2) Chakraborty, P.; Hiom, K. DHX9-Dependent Recruitment of BRCA1 to RNA Promotes DNA End Resection in Homologous Recombination. *Nat. Commun.* **2021**, *12* (1), 4126.
- (3) Lam, F. C.; Kong, Y. W.; Yaffe, M. B. Inducing DNA Damage through R-Loops to Kill Cancer Cells. *Mol. Cell. Oncol.* **2021**, *8* (1), 1848233.
- (4) Castro, J.; Daniels, M. H.; Brennan, D.; Johnston, B.; Gotur, D.; Lee, Y.-T.; Knochenhauer, K. E.; Lu, C.; Wu, J.; Nayak, S.; Collins, C.; Bansal, R.; Buker, S. M.; Case, A.; Liu, J.; Yao, S.; Sparling, B. A.; Sickmier, E. Allen.; Silver, S. J.; Blakemore, S. J.; Boriack-Sjodin, P. A.; Duncan, K. W.; Ribich, S.; Copeland, R. A. A Potent, Selective, Small-Molecule Inhibitor of DHX9 Abrogates Proliferation of Microsatellite Instable Cancers with Deficient Mismatch Repair. *Cancer Res.* **2025**, *85*, 758–776.
- (5) Aktaş, T.; Avşar İlk, İ.; Maticzka, D.; Bhardwaj, V.; Pessoa Rodrigues, C.; Mittler, G.; Manke, T.; Backofen, R.; Akhtar, A. DHX9 Suppresses RNA Processing Defects Originating from the Alu Invasion of the Human Genome. *Nature* **2017**, *544* (7648), 115–119.
- (6) Castro, J.; Ribich, S.; Brennan, D. International Patent. WO2024/220373, 2024.
- (7) Elbarbary, R. A.; Maquat, L. E. Distinct Mechanisms Obviate the Potentially Toxic Effects of Inverted-Repeat Alu Elements on Cellular RNA Metabolism. *Nat. Struct. Mol. Biol.* **2017**, *24* (6), 496–498.
- (8) Liu, S.; He, L.; Wu, J.; Wu, X.; Xie, L.; Dai, W.; Chen, L.; Xie, F.; Liu, Z. DHX9 Contributes to the Malignant Phenotypes of Colorectal Cancer via Activating NF- κ B Signaling Pathway. *Cell. Mol. Life Sci.* **2021**, *78* (24), 8261–8281.
- (9) Murayama, T.; Nakayama, J.; Jiang, X.; Miyata, K.; Morris, A. D.; Cai, K. Q.; Prasad, R. M.; Ma, X.; Efimov, A.; Belani, N.; Gerstein, E. R.; Tan, Y.; Zhou, Y.; Kim, W.; Maruyama, R.; Campbell, K. S.; Chen, L.; Yang, Y.; Balachandran, S.; Cañadas, I. Targeting DHX9 Triggers Tumor-Intrinsic Interferon Response and Replication Stress in Small Cell Lung Cancer. *Cancer Discovery* **2024**, *14* (3), 468–491.
- (10) Huang, T.-T.; Chiang, C.-Y.; Nair, J. R.; Wilson, K. M.; Cheng, K.; Lee, J.-M. AKT1 Interacts with DHX9 to Mitigate R Loop–Induced Replication Stress in Ovarian Cancer. *Cancer Res.* **2024**, *84* (6), 887–904.
- (11) Lee, T.; Paquet, M.; Larsson, O.; Pelletier, J. Tumor Cell Survival Dependence on the DHX9 DExH-Box Helicase. *Oncogene* **2016**, *35* (39), S093–S105.
- (12) Gotur, D.; Case, A.; Liu, J.; Sickmier, E. A.; Holt, N.; Knochenhauer, K. E.; Yao, S.; Lee, Y.-T.; Copeland, R. A.; Buker, S. M.; Boriack-Sjodin, P. A. Development of Assays to Support Identification and Characterization of Modulators of DExH-Box Helicase DHX9. *SLAS Discovery* **2023**, *28* (8), 376–384.
- (13) Lee, Y.-T.; Sickmier, E. A.; Grigoriu, S.; Castro, J.; Boriack-Sjodin, P. A. Crystal Structures of the DE x H-Box RNA Helicase DHX9. *Acta Crystallogr. Sect. Struct. Biol.* **2023**, *79* (11), 980–991.
- (14) Pascoe, D. J.; Ling, K. B.; Cockroft, S. L. The Origin of Chalcogen-Bonding Interactions. *J. Am. Chem. Soc.* **2017**, *139* (42), 15160–15167.
- (15) Hallenbeck, K.; Turner, D.; Renslo, A.; Arkin, M. Targeting Non-Catalytic Cysteine Residues Through Structure-Guided Drug Discovery. *Curr. Top. Med. Chem.* **2016**, *17* (1), 4–15.
- (16) Huang, F.; Han, X.; Xiao, X.; Zhou, J. Covalent Warheads Targeting Cysteine Residue: The Promising Approach in Drug Development. *Molecules* **2022**, *27* (22), 7728.
- (17) Wilcken, R.; Zimmermann, M. O.; Lange, A.; Joerger, A. C.; Boeckler, F. M. Principles and Applications of Halogen Bonding in Medicinal Chemistry and Chemical Biology. *J. Med. Chem.* **2013**, *56* (4), 1363–1388.
- (18) Buker, S. M.; Boriack-Sjodin, P. A.; Copeland, R. A. Enzyme–Inhibitor Interactions and a Simple, Rapid Method for Determining Inhibition Modality. *SLAS Discovery* **2019**, *24* (5), S15–S22.
- (19) Ishikawa, M.; Hashimoto, Y. Improvement in Aqueous Solubility in Small Molecule Drug Discovery Programs by Disruption of Molecular Planarity and Symmetry. *J. Med. Chem.* **2011**, *54* (6), 1539–1554.
- (20) Garrison, K. L.; Sahin, S.; Benet, L. Z. Few Drugs Display Flip-Flop Pharmacokinetics and These Are Primarily Associated with Classes 3 and 4 of the BDDCS. *J. Pharm. Sci.* **2015**, *104* (9), 3229–3235.
- (21) Heuser, A.; Abdul Rahman, W.; Bechter, E.; Blank, J.; Buhr, S.; Erdmann, D.; Fontana, P.; Mermet-Meillon, F.; Meyerhofer, M.; Strang, R.; Schropp, M.; Zimmermann, C.; Cortes-Cros, M.; Möbitz, H.; Hamon, J. Challenges for the Discovery of Non-Covalent WRN Helicase Inhibitors. *ChemMedChem* **2024**, *19* (8), No. e202300613.
- (22) Kwong, A. D.; Rao, B. G.; Jeang, K.-T. Viral and Cellular RNA Helicases as Antiviral Targets. *Nat. Rev. Drug Discovery* **2005**, *4* (10), 845–853.
- (23) Nguyen, G. H.; Dexheimer, T. S.; Rosenthal, A. S.; Chu, W. K.; Singh, D. K.; Mosedale, G.; Bachrati, C. Z.; Schultz, L.; Sakurai, M.; Savitsky, P.; Abu, M.; McHugh, P. J.; Bohr, V. A.; Harris, C. C.; Jadhav, A.; Gileadi, O.; Maloney, D. J.; Simeonov, A.; Hickson, I. D. A Small Molecule Inhibitor of the BLM Helicase Modulates Chromosome Stability in Human Cells. *Chem. Biol.* **2013**, *20* (1), 55–62.
- (24) Wever, M. J. A.; Scommegna, F. R.; Egea-Rodriguez, S.; Dehghani-Tafti, S.; Brandao-Neto, J.; Poisson, J.-F.; Helfrich, I.; Antson, A. A.; Rodeschini, V.; Bax, B.; Roche, D.; Sanders, C. M. Structure-Based Discovery of First Inhibitors Targeting the Helicase Activity of Human PIF1. *Nucleic Acids Res.* **2024**, *52* (20), 12616–12632.
- (25) Bol, G. M.; Xie, M.; Raman, V. DDX3, a Potential Target for Cancer Treatment. *Mol. Cancer* **2015**, *14* (1), 188.
- (26) Papillon, J. P. N.; Nakajima, K.; Adair, C. D.; Hempel, J.; Jouk, A. O.; Karki, R. G.; Mathieu, S.; Möbitz, H.; Ntaganda, R.; Smith, T.; Visser, M.; Hill, S. E.; Hurtado, F. K.; Chenail, G.; Bhang, H.-E. C.; Bric, A.; Xiang, K.; Bushold, G.; Gilbert, T.; Vattay, A.; Dooley, J.; Costa, E. A.; Park, I.; Li, A.; Farley, D.; Lounkine, E.; Yue, Q. K.; Xie, X.; Zhu, X.; Kulathila, R.; King, D.; Hu, T.; Vulic, K.; Cantwell, J.; Luu, C.; Jagani, Z. Discovery of Orally Active Inhibitors of Brahma Homolog (BRM)/SMARCA2 ATPase Activity for the Treatment of Brahma Related Gene 1 (BRG1)/SMARCA4-Mutant Cancers. *J. Med. Chem.* **2018**, *61* (22), 10155–10172.
- (27) Moradei, O.; Lampe, J.; Harvey, D.; Campbell, J.; Duncan, K.; Munchhof, M. International Patent. WO2020/023657, 2020.
- (28) Kofink, C.; Trainor, N.; Mair, B.; Wöhrle, S.; Wurm, M.; Mischerikow, N.; Roy, M. J.; Bader, G.; Greb, P.; Garavel, G.; Diers, E.; McLennan, R.; Whitworth, C.; Vetma, V.; Rumpel, K.; Scharnweber, M.; Fuchs, J. E.; Gerstberger, T.; Cui, Y.; Gremel, G.; Chetta, P.; Hopf, S.; Budano, N.; Rinnenthal, J.; Gmaschitz, G.; Mayer, M.; Koegl, M.; Ciulli, A.; Weinstabl, H.; Farnaby, W. A Selective and Orally Bioavailable VHL-Recruiting PROTAC Achieves SMARCA2 Degradation in Vivo. *Nat. Commun.* **2022**, *13* (1), 5969.
- (29) Baltgalvis, K. A.; Lamb, K. N.; Symons, K. T.; Wu, C.-C.; Hoffman, M. A.; Snead, A. N.; Song, X.; Glaza, T.; Kikuchi, S.; Green, J. C.; Rogness, D. C.; Lam, B.; Rodriguez-Aguirre, M. E.; Woody, D. R.; Eissler, C. L.; Rodiles, S.; Negron, S. M.; Bernard, S. M.; Tran, E.; Pollock, J.; Tabatabaei, A.; Contreras, V.; Williams, H. N.; Pastuszka, M. K.; Sigler, J. J.; Pettazzoni, P.; Rudolph, M. G.; Classen, M.; Brugger, D.; Claiborne, C.; Plancher, J.-M.; Cuartas, I.; Seoane, J.; Burgess, L. E.; Abraham, R. T.; Weinstein, D. S.; Simon, G. M.; Patricelli, M. P.; Kinsella, T. M. Chemoproteomic Discovery of a Covalent Allosteric Inhibitor of WRN Helicase. *Nature* **2024**, *629* (8011), 435–442.
- (30) Parker, M. J.; Lee, H.; Yao, S.; Irwin, S.; Hwang, S.; Belanger, K.; De Mare, S. W.; Surgenor, R.; Yan, L.; Gee, P.; Morla, S.; Puyang,

X.; Hsiao, P.; Zeng, H.; Zhu, P.; Korpai, M.; Dransfield, P.; Bolduc, D. M.; Larsen, N. A. Identification of 2-Sulfonyl/Sulfonamide Pyrimidines as Covalent Inhibitors of WRN Using a Multiplexed High-Throughput Screening Assay. *Biochemistry* **2023**, *62* (14), 2147–2160.

(31) Picco, G.; Rao, Y.; Al Saedi, A.; Lee, Y.; Vieira, S. F.; Bhosle, S.; May, K.; Herranz-Ors, C.; Walker, S. J.; Shenje, R.; Dincer, C.; Gibson, F.; Banerjee, R.; Hewitson, Z.; Werner, T.; Cottom, J. E.; Peng, Y.; Deng, N.; Zhang, Y.; Nartey, E. N.; Nickels, L.; Landis, P.; Conticelli, D.; McCarten, K.; Bush, J.; Sharma, M.; Lightfoot, H.; House, D.; Milford, E.; Grant, E. K.; Glogowski, M. P.; Wagner, C. D.; Bantscheff, M.; Rutkowska-Klute, A.; Cell Model Network UK Group; Zappacosta, F.; Pettinger, J.; Barthorpe, S.; Eberl, H. C.; Jones, B. T.; Schneck, J. L.; Murphy, D. J.; Voest, E. E.; Taygerly, J. P.; DeMartino, M. P.; Coelho, M. A.; Houseley, J.; Sharma, G.; Schwartz, B.; Garnett, M. J. Novel WRN Helicase Inhibitors Selectively Target Microsatellite-Unstable Cancer Cells. *Cancer Discovery* **2024**, *14* (8), 1457–1475.

(32) Ferretti, S.; Hamon, J.; De Kanter, R.; Scheufler, C.; Andraos-Rey, R.; Barbe, S.; Bechter, E.; Blank, J.; Bordas, V.; Dammasa, E.; Decker, A.; Di Nanni, N.; Dourdoigne, M.; Gavioli, E.; Hattenberger, M.; Heuser, A.; Hemmerlin, C.; Hinrichs, J.; Kerr, G.; Laborde, L.; Jaco, L.; Núñez, E. J.; Martus, H.-J.; Quadt, C.; Reschke, M.; Romanet, V.; Schaeffer, F.; Schoepfer, J.; Schrapp, M.; Strang, R.; Voshol, H.; Wartmann, M.; Welly, S.; Zéciri, F.; Hofmann, F.; Möbitz, H.; Cortés-Cros, M. Discovery of WRN Inhibitor HRO761 with Synthetic Lethality in MSI Cancers. *Nature* **2024**, *629* (8011), 443–449.

(33) Malo, N.; Hanley, J. A.; Cerquozzi, S.; Pelletier, J.; Nadon, R. Statistical Practice in High-Throughput Screening Data Analysis. *Nat. Biotechnol.* **2006**, *24* (2), 167–175.

(34) Jagtap, P. K. A.; Müller, M.; Kiss, A. E.; Thomae, A. W.; Lapouge, K.; Beck, M.; Becker, P. B.; Hennig, J. Structural Basis of RNA-Induced Autoregulation of the DExH-Type RNA Helicase Maleless. *Mol. Cell* **2023**, *83* (23), 4318–4333.

(35) Koh, H. R.; Xing, L.; Kleiman, L.; Myong, S. Repetitive RNA Unwinding by RNA Helicase A Facilitates RNA Annealing. *Nucleic Acids Res.* **2014**, *42* (13), 8556–8564.

(36) Knockenhauer, K. E.; Copeland, R. A. The Importance of Binding Kinetics and Drug–Target Residence Time in Pharmacology. *Br. J. Pharmacol.* **2024**, *181* (21), 4103–4116.

(37) Copeland, R. A.; Pompliano, D. L.; Meek, T. D. Drug–Target Residence Time and Its Implications for Lead Optimization. *Nat. Rev. Drug Discovery* **2006**, *5* (9), 730–739.

(38) Lu, H.; Tonge, P. J. Drug–Target Residence Time: Critical Information for Lead Optimization. *Curr. Opin. Chem. Biol.* **2010**, *14* (4), 467–474.

(39) McCoy, A. J.; Grosse-Kunstleve, R. W.; Adams, P. D.; Winn, M. D.; Storoni, L. C.; Read, R. J. Phaser Crystallographic Software. *J. Appl. Crystallogr.* **2007**, *40* (4), 658–674.

(40) Emsley, P.; Lohkamp, B.; Scott, W. G.; Cowtan, K. Features and Development of Coot. *Acta Crystallogr. D Biol. Crystallogr.* **2010**, *66* (4), 486–501.

(41) Murshudov, G. N.; Vagin, A. A.; Dodson, E. J. Refinement of Macromolecular Structures by the Maximum-Likelihood Method. *Acta Crystallogr. D Biol. Crystallogr.* **1997**, *53* (3), 240–255.